NATIONAL ENERGY TECHNOLOGY LABORATORY

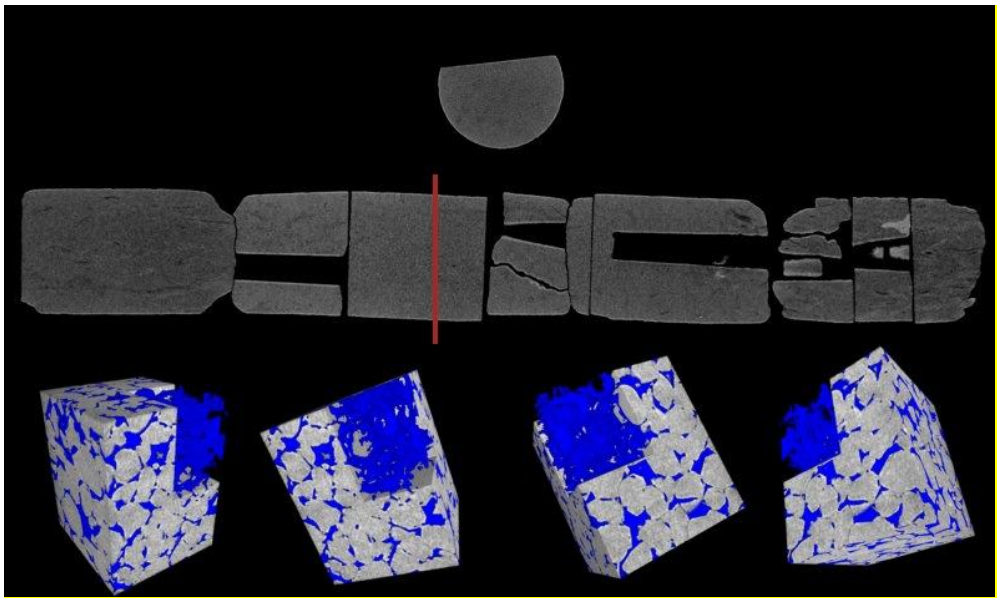

Computed Tomography Scanning and Petrophysical Measurements of the Lively Grove #1 Well Core

12 July 2023

U.S. DEPARTMENT OF ENERGY | NATIONAL ENERGY TECHNOLOGY LABORATORY

Office of Fossil Energy and Carbon Management

DOE/NETL-2023/3877

Disclaimer

Cover Illustration: Top: cross-sectional image of medical computed tomography (CT) scan of section from Lively Grove #1 Well core, depths of 3,665 to 3,667 ft. Bottom: four representations of isolated pore space (blue) from micro-CT scans, at a resolution of 1.51 μm^3, of core from a depth of 3,666 ft.

Suggested Citation: Crandall, D.; Paronish, T.; Mitchell, N.; Jarvis, K.; Brown, S.; Moore, J.; Gill, M.; Blakley, C.; Okwen, R.; Korose, C.; Carman, C. *Computed Tomography Scanning and Petrophysical Measurements of the Lively Grove #1 Well Core;* DOE/NETL-2023/3877; NETL Technical Report Series; U.S. Department of Energy, National Energy Technology Laboratory: Morgantown, WV, 2023; p 60. DOI: https://doi.org/10.2172/1989188.

An electronic version of this report can be found at:

https://edx.netl.doe.gov/group/core-characterization
https://netl.doe.gov/energy-analysis/search

The data in this report can be accessed from NETL's Energy Data eXchange (EDX) online system (https://edx.netl.doe.gov) using the following link:

https://edx.netl.doe.gov/dataset/isgs-carbonsafe-lively-grove-core

Computed Tomography Scanning and Petrophysical Measurements of the Lively Grove #1 Well Core

Dustin Crandall[1], Thomas Paronish[1,2], Natalie Mitchell[1,2], Karl Jarvis[1,2], Sarah Brown[1,2], Johnathan Moore[1], Magdalena Gill[1,2], Curt Blakley[3], Roland Okwen[3], Christopher Korose[3], Carl Carman[3]

[1]U.S. Department of Energy, National Energy Technology Laboratory, 3610 Collins Ferry Road, Morgantown, WV 26507

[2]NETL Support Contractor, 3610 Collins Ferry Road, Morgantown, WV 26507

[3]Illinois State Geological Survey, 615 E Peabody Drive, Champaign, IL 61820

DOE/NETL-2023/3877

12 July 2023

NETL Contacts:

Dustin Crandall, Principal Investigator and Technical Portfolio Lead

Bryan Morreale, Associate Laboratory Director for Research & Innovation Center, Research & Innovation Center

This page intentionally left blank.

Table of Contents

List of Figures

List of Figures (cont.)

List of Tables

Acronyms, Abbreviations, and Symbols

Term	Description
2D	Two-dimensional
3D	Three-dimensional
CO_2	Carbon dioxide
CarbonSAFE	Carbon Storage Assurance Facility Enterprise
CT	Computed tomography
CTN	CT number
d	Sample thickness
DOE	Department of Energy
EDX	NETL's Energy Data eXchange
HU	Hounsfield Unit
H	External magnetic field
I	Measured Intensity
ISGS	Illinois State Geological Survey
I_0	Source Intensity
J	Magnetic response (per unit volume)
k	Volume susceptibility
LG #1	Lively Grove #1 Well
MSCL	Multi-Sensor Core Logger
NETL	National Energy Technology Laboratory
PSEC	Prairie State Energy Campus
XRF	X-ray fluorescence
μ	Compton attenuation coefficient
ρ	Bulk Density

Acknowledgments

This work was completed at the National Energy Technology Laboratory (NETL) with support from the U.S. Department of Energy's (DOE) Office of Fossil Energy Oil & Gas Program. The authors wish to acknowledge Bryan Morreale (NETL Research & Innovation Center), Mark McKoy (NETL Technology Development and Integration Center), and Darin Damiani (DOE Office of Fossil Energy) for programmatic guidance, direction, and support.

The authors would like to thank Scott Workman and Bryan Tennant for computed tomography data collection and technical support. Thank you to the staff of the Geologic Characterization, Analytics, and Modeling laboratory at NETL for continued laboratory support.

ABSTRACT

The computed tomography (CT) facilities and the Multi-Sensor Core Logger (MSCL) at the National Energy Technology Laboratory (NETL) in Morgantown, West Virginia were used to characterize core from the Lively Grove #1 Well (API 121892494700), drilled near Marissa, Washington County, Illinois. Core from the well was obtained as part of the Illinois Storage Corridor's Carbon Storage Assurance Facility Enterprise (CarbonSAFE) project (DE-FE0031892).

The primary impetus of this work was to capture a detailed digital representation of the core from the Lively Grove #1 Well. The collaboration between the U.S. Department of Energy's (DOE) NETL and the Illinois State Geological Survey (ISGS) enables other research entities to access information about this potential carbon storage location and Cambro-Ordovician Storage Complex formations of the Illinois Basin. The resultant datasets are presented in this report and can be accessed from NETL's Energy Data eXchange (EDX) online system using the following link: https://edx.netl.doe.gov/dataset/isgs-carbonsafe-lively-grove-core.

All equipment and techniques used were non-destructive, enabling future examinations and analyses to be performed on these cores. Fractures, discontinuities, and millimeter-scale features were readily detectable with the medical CT scanner-acquired images. Imaging with the NETL medical CT scanner was performed on entire cores. Qualitative analysis of the medical CT images, coupled with X-ray fluorescence (XRF), gamma density, and magnetic susceptibility measurements from the MSCL were useful in identifying zones of interest for potential future analysis. Higher-resolution industrial and micro-CT images were acquired from selected zones along the depth of the core to visualize the structure in higher detail. The ability to quickly identify key areas for more detailed study with higher resolution will save time and resources in future studies. The combination of methods used provides a multi-scale analysis of the core; with the resulting macro- and micro-descriptions relevant to many subsurface energy related examinations traditionally performed at NETL.

1. INTRODUCTION

Evaluation of reservoir and caprock samples can support resource estimations for geologic carbon dioxide (CO_2) storage. While it is common for commercial entities to perform these characterizations, the resources necessary to conduct these analyses are not always available to the broader interest base, such as state agencies and research-based consortia. To meet the growing need for comprehensive and high-quality lithologic data for collaborative research initiatives, the U.S. Department of Energy's (DOE) National Energy Technology Laboratory (NETL) has used available resources to develop a systematic approach for the evaluation of subsurface geological core materials.

In this study, the primary objective was to characterize core with methods not available to most researchers. The data is presented in several formats here and online at NETL's Energy Data eXchange (EDX) (https://edx.netl.doe.gov/dataset/isgs-carbonsafe-lively-grove-core). These data are potentially useful for various analyses. However, little detailed analysis is presented in this report as the research objective was not to perform a site characterization, but rather to acquire the data for others to utilize and to create a digital representation of the core that could be preserved in perpetuity. A lengthy and robust core analysis was performed by Illinois State Geological Survey (ISGS) as part of the DOE-funded project DE-FE0031892 that can be reviewed for a more complete understanding of the formations of interest in the Illinois Basin.

1.1 SITE BACKGROUND

The Lively Grove #1 Well (LG #1) was drilled in association with the Illinois Storage Corridor's Carbon Storage Assurance Facility Enterprise (CarbonSAFE) Phase III project with the ultimate goal of sequestration of CO_2 from the Prairie State Energy Campus (PSEC). The LG #1 was drilled in Lively Grove township in Washington County, Illinois, north-northeast of the PSEC site in the summer of 2021 to a total depth of 5,890 ft (Figure 1). The well was drilled to characterize reservoir and confining formations for the injection of CO_2 into a stacked reservoir (St. Peter Sandstone and Potosi Dolomite), with the Maquoketa Shale as the primary seal (Whittaker, 2022).

The LG #1 (API 121892494700) acquired whole core in the Maquoketa, St. Peter, and Knox Dolomite Megagroup. The well sits about 6 miles north of the PSEC plant (Lat: 38.352151/Long: -89.644768) and is geologically located on the western edge of the Illinois Basin depocenter (Whittaker, 2022).

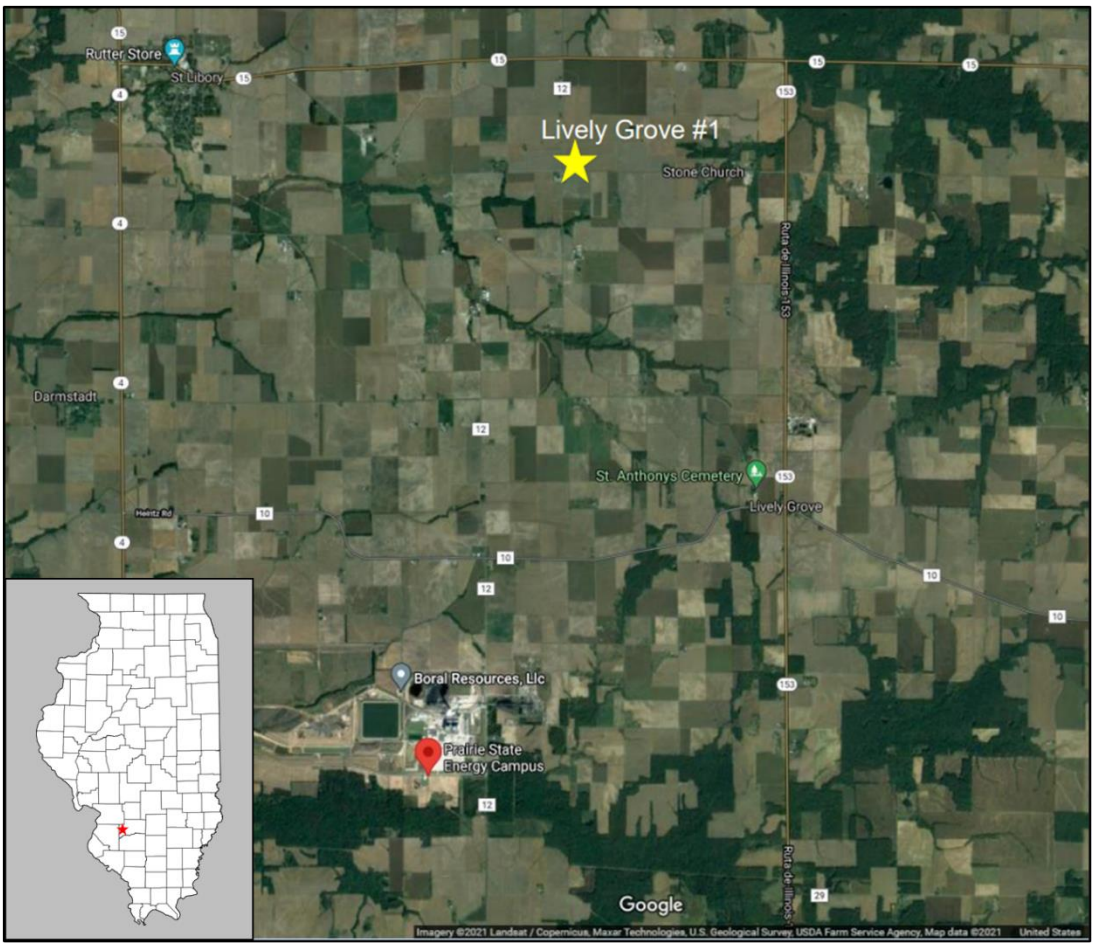

Figure 1: Site map for Lively Grove #1 Well (yellow star) and Prairie State Energy Campus (red pin).

1.2 CORE DESCRIPTION

The LG #1 cores include rock from the Maquoketa, Joachim Formation, St. Peter Formation, and Knox Group (Potosi Dolomite).

The Maquoketa Shale (2,885 to 2,945.8 ft) is made up of gray to light-gray shale with some thinly interbedded intervals of limestone. The Joachim Formation (3,570 to 3,587.8 ft) is made up of light-gray mudstone to wackestone with thinly interbedded intervals of gray to dark-gray clay-rich mudstone. The St. Peter Formation (3,587 to 3,597 ft and 3,649 to 3,675 ft) is made up of a tannish-white, fine- to very fine-grained sandstone with prominent vertical burrowing. The Knox Group (Potosi Dolomite) (4,885 to 4,912 ft and 5,294 to 5,317 ft) is made up of a light-grey dolomite that has some vertical to sub-vertical fracturing and zones of mm- to cm-scale vuggy porosity.

During transport to NETL core was lost and damaged; specifically six 2/3 core sections from 4,899.2 to 5,311.6 ft were lost, in addition to 1/3 slabbed core from 3,669 to 3,674.5 ft and 5,294 to 5,304 ft. Scanning was performed on available sections, however, gaps in the data due to missing core do exist and are mentioned in the text where relevant.

1.3 CORE PHOTOGRAPHS

Figure 2 to 11 are core photographs of the 4-in. diameter LG #1 core.

Maquoketa Shale:

Figure 2: Photographs of the LG #1 core from 2,885.5–2,905 ft.

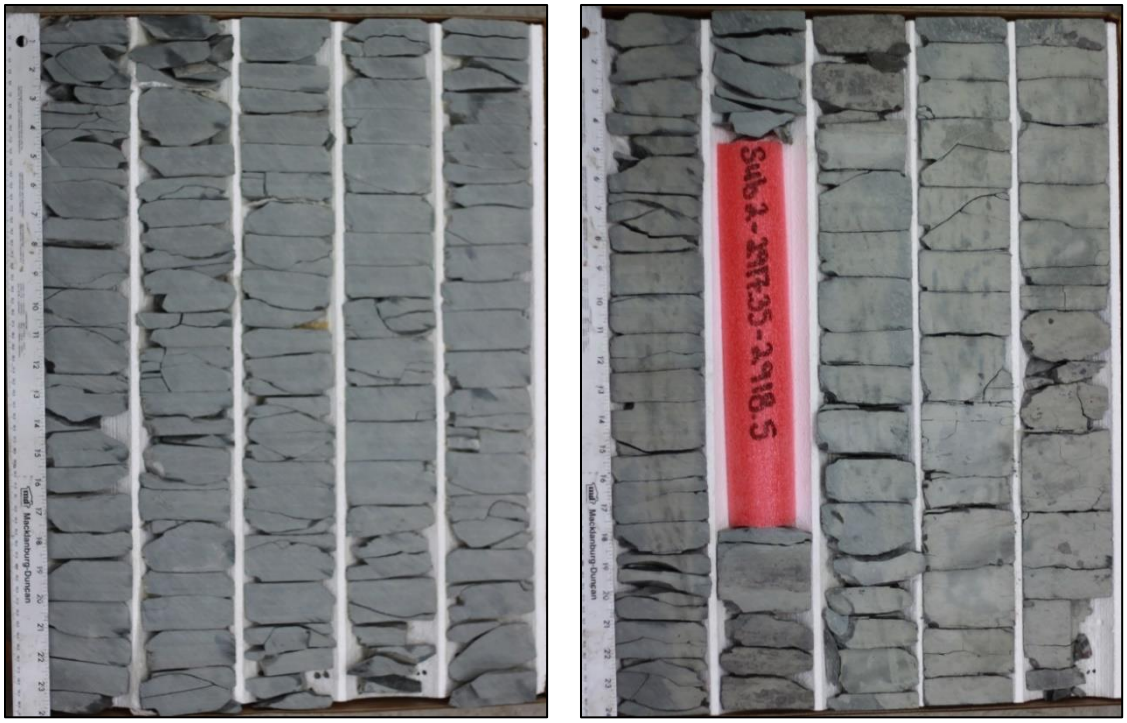

Figure 3: Photographs of the LG #1 core from 2,905–2,925 ft.

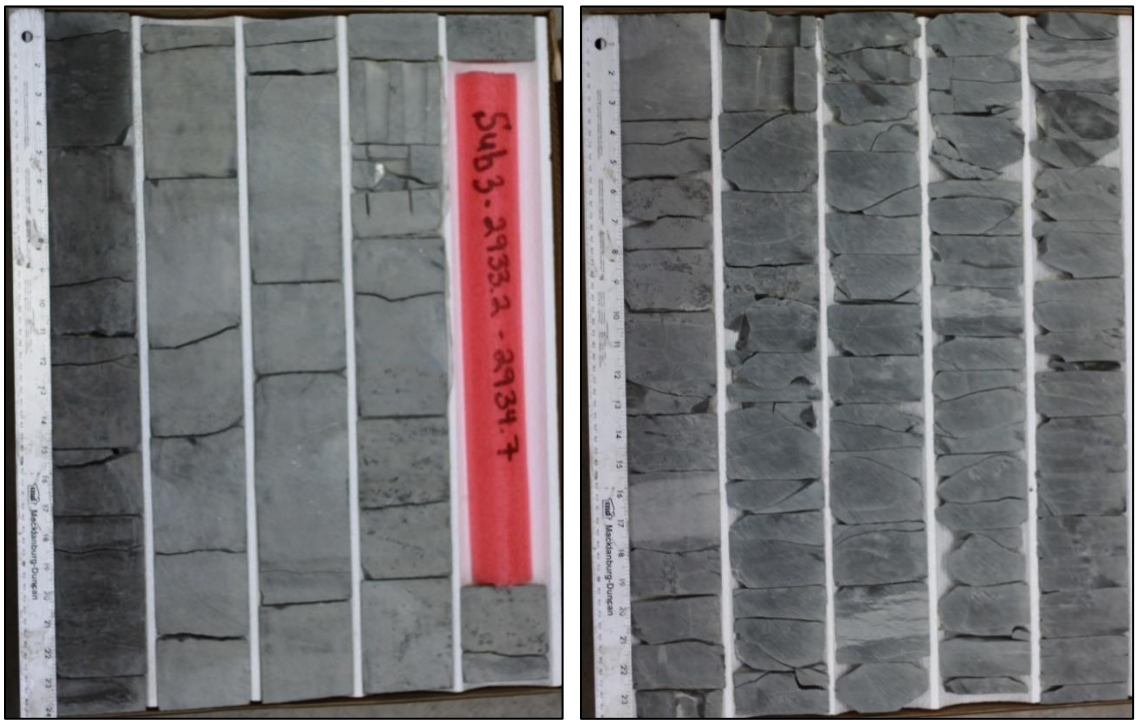

Figure 4: Photographs of the LG #1 core from 2,925–2,945 ft.

Figure 5: Photographs of the LG #1 core from 2,945–2,945.8 ft.

Joachim Formation:

Figure 6: Photographs of the LG #1 core from 3,570–3,590 ft.

St. Peter Sandstone:

Figure 7: Photographs of the LG #1 core from 3,590–3,597.11 ft.

Figure 8: Photographs of the LG #1 core from 3,649–3,669 ft.

Knox Megagroup:

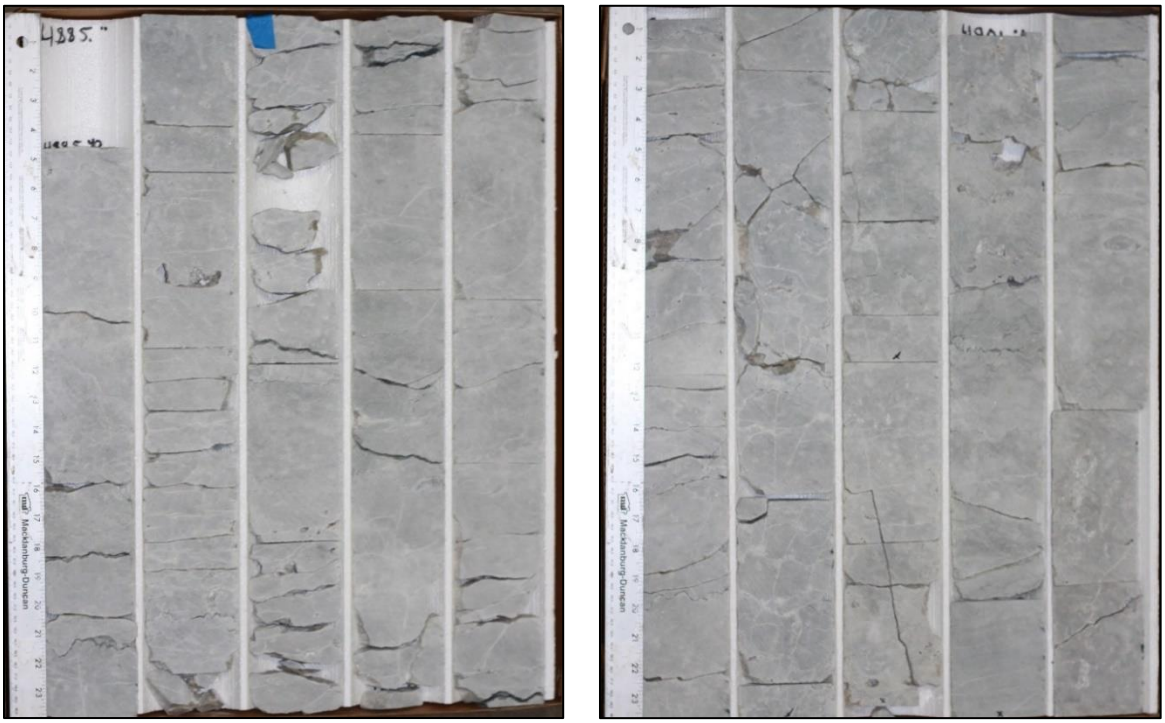

Figure 9: Photographs of the LG #1 core from 4,885.4–4,905 ft.

Figure 10: Photographs of the LG #1 core from 4,905–4,911.56 ft.

Figure 11: Photographs of the LG #1 core from 5,304–5,316 ft.

2. DATA ACQUISITION AND METHODOLOGY

The core was evaluated using medical computed tomography (CT) scanning and high spatial resolution geophysical measurements along its length, including X-ray fluorescence (XRF) spectrometry.

2.1 MEDICAL CT SCANNING

Core scale CT scanning was performed with a Toshiba Aquilion TSX-101A/R medical CT scanner shown in Figure 12. The medical CT scanner generates images with a resolution in the millimeter range, with scans having voxel resolutions of 0.43 x 0.43 mm in the XY plane and 0.50 mm along the core's long axis (i.e., z-axis). The scans were conducted at a voltage of 135 kV and at a current of 200 mA. Subsequent processing and combining of stacks were performed to create three-dimensional (3D) volumetric representations of the cores and a two-dimensional (2D) cross-section through the middle of the core samples using ImageJ, an open-source image processing software package (Schneider et al., 2012). The variation in greyscale values observed in the CT images indicates changes in the CT number (CTN) obtained from the CT scans, which is directly proportional to changes in the attenuation and density of the scanned rock; darker regions are less dense. Filled fractures, open fractures, and changes in bedding structure can all be resolved via careful examination of the CT images (Figures 18–35). While the medical CT scanner was not used for detailed characterization in this study, it allowed for non-destructive bulk characterization of the core.

Figure 12: Toshiba Aquilion Multislice Helical CT scanner at NETL used for core analysis.

2.2 INDUSTRIAL CT SCANNING

High-resolution CT scans were performed on intervals of interest using NETL's North Star Imaging Inc. M-5000® Industrial Computed Tomography System (Figure 13). The system is used to obtain higher resolution scans, resolving some unclear features from the medical scans.

The scans were performed at varying voltages and currents to provide a balance between resolution and a sufficient sample penetration for each sample. 2D radiographs of the samples were obtained 1,440 times while rotating 360°, or at every 0.25°. Radiographs were comprised of 10 images averaged with a 5 s acquisition for each image to ensure sufficient image contrast.

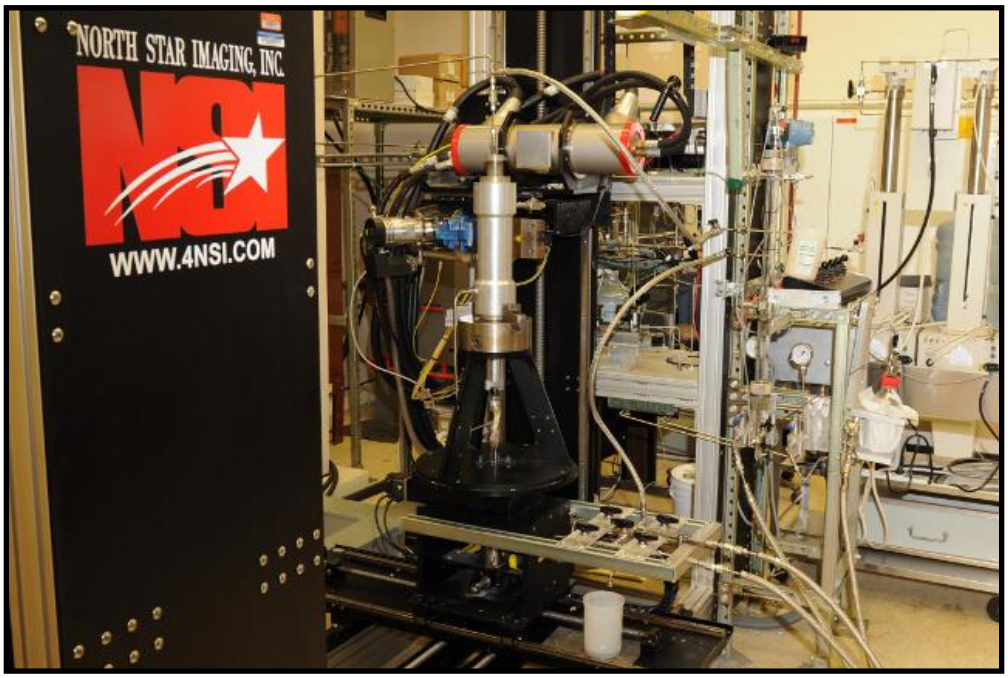

Figure 13: North Star Imaging Inc. M-5000 ® Industrial Computed Tomography Scanner at NETL used for core analysis.

2.3 MICRO-CT SCANNING

Micro-CT scanning was performed using two scanners: a ZEISS Xradia MicroXCT-400 scanner and a TESCAN DynaTOM micro-CT scanner. The DynaTOM performs both dynamic and static imaging while capturing scans of sub-mm to cm-scale samples (Figure 14). The Xradia system has the highest resolution of the scanners at NETL and scans samples sizes from sub-mm to 25 mm (Figure 15). Both scanners provide detailed image data that can be used to infer porosity, mineralogy, and structure.

Figure 14: TESCAN DynaTOM Micro-CT scanner used for high-resolution CT imaging at NETL.

Figure 15: Zeiss Xradia MicroXCT-400 Micro-CT scanner used for high-resolution CT imaging at NETL.

2.4 CORE LOGGING

Geophysical measurements of magnetic susceptibility and attenuated gamma counts were obtained with a Geotek® Multi-Sensor Core Logging (MSCL) system on competent sections of the LG #1 core and are reported in Section 3.4. Additionally, the system measured bulk elemental chemistry using a built-in, portable XRF spectrometer. The compiled core logs were scaled to fit on single pages for rapid review of the combined data from the medical CT scans and XRF readings. Core scale CT scanning was done with NETL's Toshiba Aquilion TSX-101A/R medical CT scanner.

2.4.1 Magnetic Susceptibility

Magnetic susceptibility is a measure of the degree of magnetization in a sample. The sample is exposed to an external magnetic field and magnetic susceptibility is its measured magnetic response to that field:

$$J = kH$$

Where, *J* is the magnetic response (per unit volume), *k* is volume susceptibility, and *H* is an external magnetic field. The measurement unit is dimensionless (abbreviated as SI).

All materials have magnetic susceptibility. Positive values of magnetic susceptibility indicate that materials are *paramagnetic* and occur in rocks that consist of the majority ferromagnetic, ferrimagnetic, or antimagnetic (iron-bearing) materials. Negative values of magnetic susceptibility indicate that materials are *diamagnetic* and occur in rocks dominated by non-iron material (e.g., calcite or quartz). Table 1 lists examples of common magnetic susceptibility ranges (Hunts et al., 1995).

Magnetic susceptibility was measured using the Bartington point sensor, where a 1-cm diameter, low intensity (8.0 A/m RMS), non-sensitive, alternating magnetic field (2 kHz) was generated for 10 s. To minimize any potential drift in the oscillating field, the point sensor was zeroed at the beginning and end of the sample and after every fifth measurement. The point sensor, due to the small field, was limited in whole core measurements and was temperature dependent (Geotek Ltd. Multi-Sensor Core Logger Manual, Version 05-10; Geotek Ltd., 2010).

2.4.2 Gamma Density

Gamma density was acquired by subjecting the sample to gamma radiation and then measuring the attenuation of that radiation. The attenuation is directly proportional to the density of the sample and is acquired by measuring the difference between radiation energy at the emission source and after it passes through the sample. Specifically, the MSCL software calculates the bulk density, ρ, by using the following equation:

$$\rho = \left(\frac{1}{\mu d}\right) \ln\left(\frac{I_o}{I}\right)$$

Where μ = Compton attenuation coefficient, d = sample thickness, I_o = source intensity, and I = measured intensity.

Table 1: Magnetic Susceptibility Values for Common Minerals (Hunts et al., 1995)

Mineral	x (*10^{-6}) SI
Water	9
Calcite	-7.5 to -39
Halite, Gypsum	-10 to -60
Shale	63 to 18,600
Illite, Montmorillonite	330 to 410
Pyrite	5 to 3,500
Chalcopyrite	23 to 400
Hematite	500 to 40,000
Magnetite	1,000,000 to 5,700,000

2.4.3 XRF Spectrometry

In addition to the geophysical measurements, a portable handheld Olympus Vanta M Series XRF Spectrometer was used to measure relative elemental abundances of aggregated "light elements" up to and including sodium, and various heavy elements which were measured individually. Elemental abundances are reported in ppm relative to the total elemental composition (i.e., the total XRF counts).

The XRF spectrometer measures elemental abundances by subjecting the sample to X-ray photons. The high energy of the photons displaces inner orbital electrons in the respective elements. The vacancies in the lower orbitals cause outer orbital electrons to "fall" into lower orbits to satisfy the disturbed electron configuration. The substitution into lower orbitals causes a release of a secondary X-ray photon, which has an energy associated with a specific element. These relative and element specific energy emissions can then be used to determine bulk elemental composition.

The Olympus Vanta M Series XRF Spectrometer used a "GeoChem(3-beam) Mode" to run at 30.48 cm (1 ft) resolution for 120 s exposure time analysis (40 s per beam). The GeoChem(3-beam) Mode utilizes a 3-beam analysis that resolves major (Mg, Al, Si, P, S, Fe, K, Ca, and Ti), minor (V, Cu, Ni, Cr, Mn, Ba, Sr, and Pb), and trace elements (Co, Zn, As, Zr, Mo, Ag, Cd, Sn, Sb, Hg, W, Th, U, and Bi), and some rare earth elements (Y, Ce, La, Pr, and Nd) (orange, Figure 16). The system also resolves an aggregated "light element" (H to Na) (green, Figure 16).

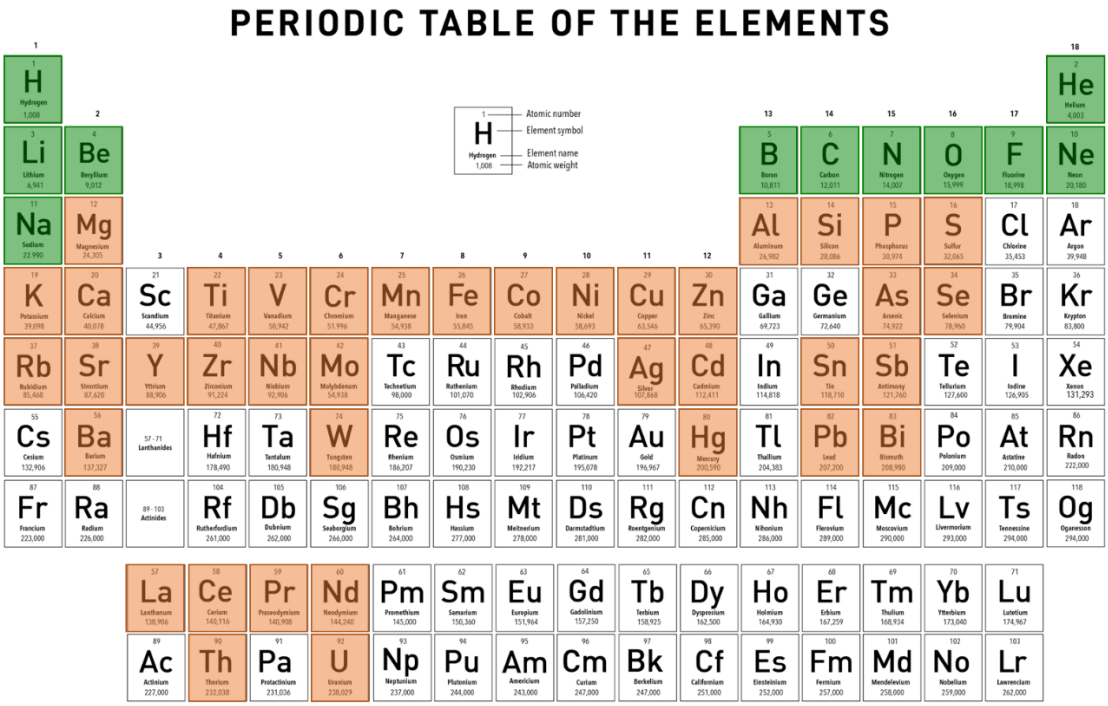

Figure 16: Periodic table showing elements measurable by the Olympus Vanta M Series XRF Spectrometer using the "GeoChem(3-beam)" mode.

2.5 DATA COMPILATION

Strater® by Golden Software was used to compile the medical CT data into a series of logs. The data used to generate these logs can be accessed from NETL's EDX online system using the following link: https://edx.netl.doe.gov/dataset/isgs-carbonsafe-lively-grove-core.

3. RESULTS

The following sections contain the data obtained from the medical, industrial, and micro-CT scanners, in addition to the MSCL scans, of the LG #1 core.

3.1 MEDICAL CT SCANS

Processed 2D slices of the medical CT scans through the cores are shown. As discussed previously, the variation in greyscale values observed in the medical CT images indicates changes in the CTN obtained, which is directly proportional to changes in the attenuation of the X-ray beam, and thus density of the scanned rock (i.e., darker regions are less dense, lighter regions are denser).

The 2/3 slabbed core was scanned in 3 ft or smaller sections. Detailed information in logbooks and photographs of the core were used to confirm the locations of missing core and depths. Due to core loss during shipping the 1/3 slabbed core was scanned in 5 ft increments over depths of 4,895 to 4,905 ft and 5,309 to 5,314 ft.

3.1.1 XZ Planes

A 2D image through the center of each core can be found in Figure 18 through Figure 35. These are referred to as "XZ" planes with the coordinates that are shown in Figure 17. Each image has a red 2-cm scale bar; the core diameter is 4 in. (10.16 cm). The labels below each 2D XZ plane in Figure 18 through Figure 35 are the depth of each core. The greyscale values were maintained for all of these images to enable comparison across formations.

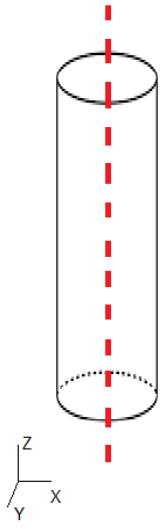

Figure 17: Schematic of the XZ isolated plane through the vertical center of the medical CT scans.

3.1.2 Lively Grove #1

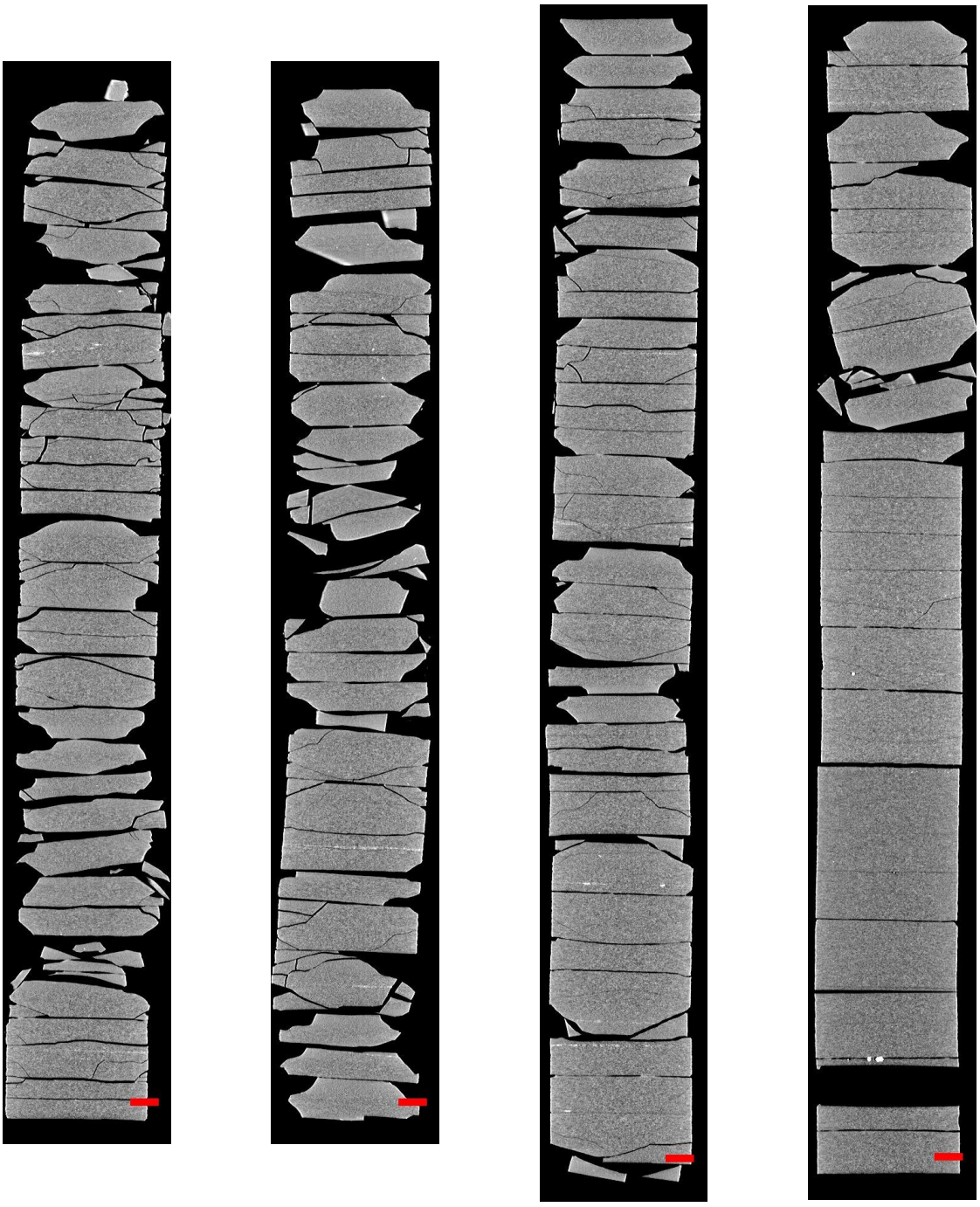

2,885–2,888 ft **2,888–2,890 ft** **2,890–2,893 ft** **2,893–2,896 ft**

Figure 18: 2D midplanes of the medical CT scans of the LG #1 core from 2,885–2,896 ft.

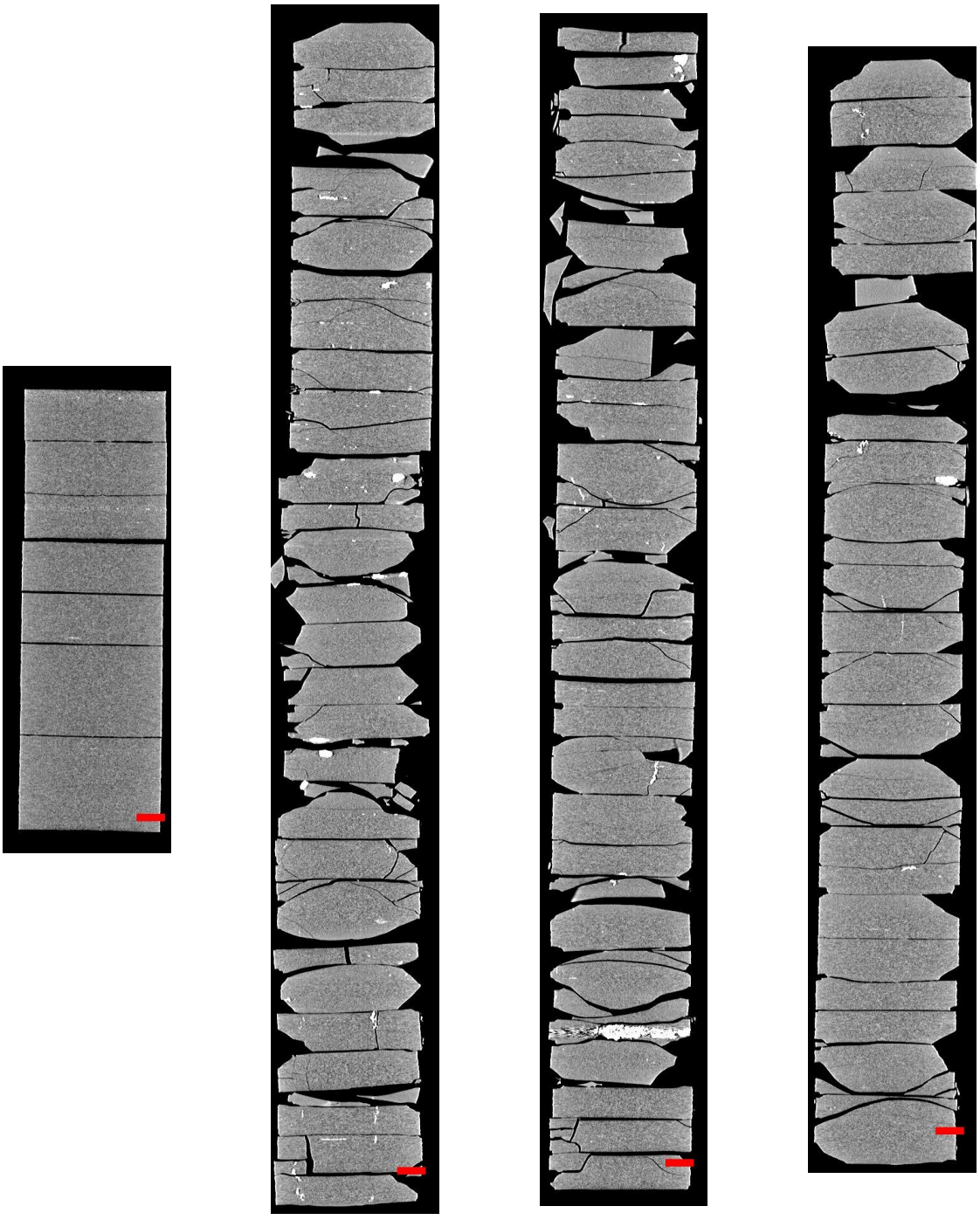

2,896–2,898 ft **2,898–2,901 ft** **2,901–2,904 ft** **2,904–2,907 ft**

Figure 19: 2D midplanes of the medical CT scans of the LG #1 core from 2,896–2,907 ft.

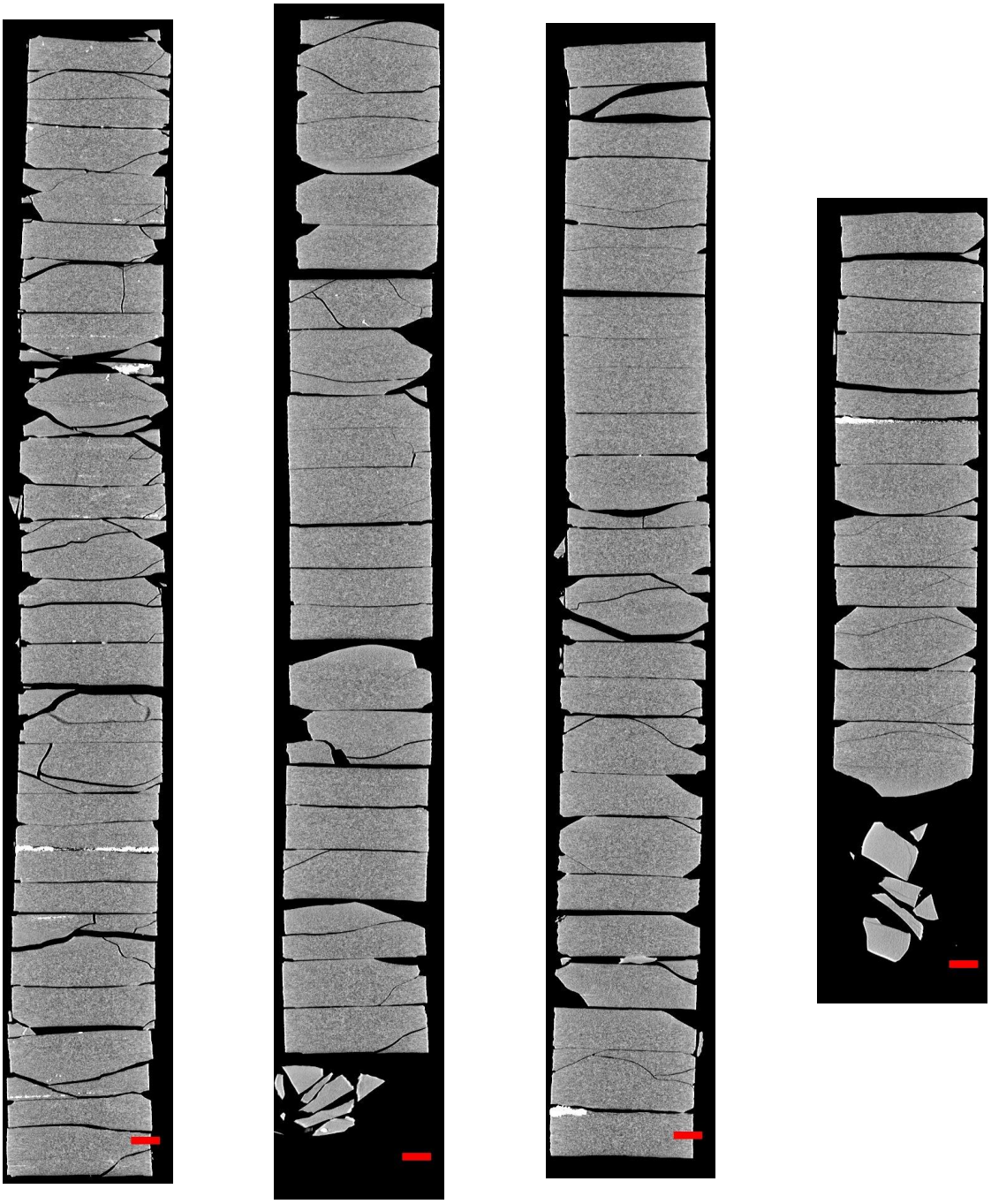

2,907–2,910 ft **2,910–2,913 ft** **2,913–2,915 ft** **2,915–2,918 ft**

Figure 20: 2D midplanes of the medical CT scans of the LG #1 core from 2,907–2,918 ft.

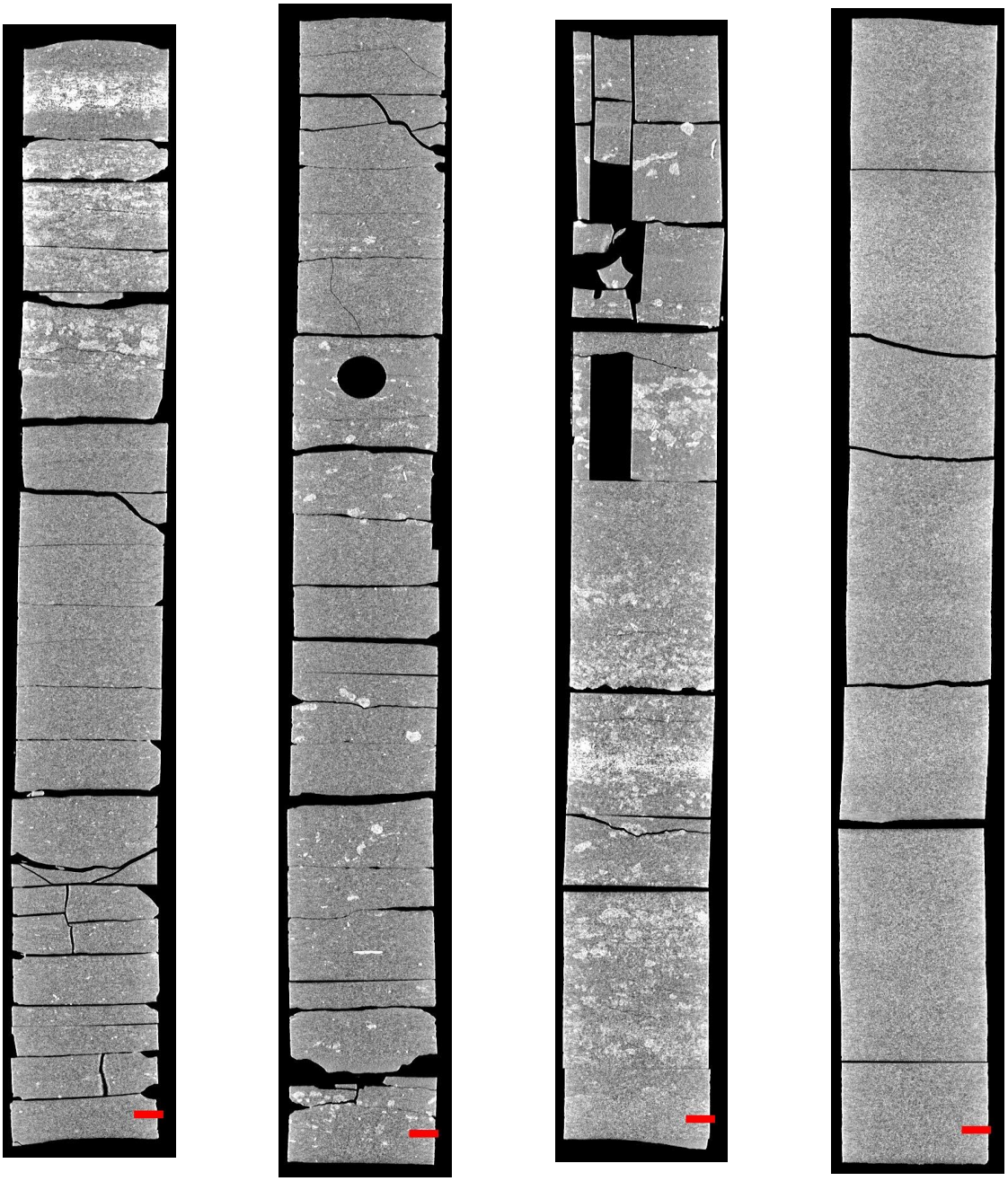

2,918–2,921 ft **2,921–2,924 ft** **2,924–2,927 ft** **2,927–2,930 ft**

Figure 21: 2D midplanes of the medical CT scans of the LG #1 core from 2,918–2,930 ft.

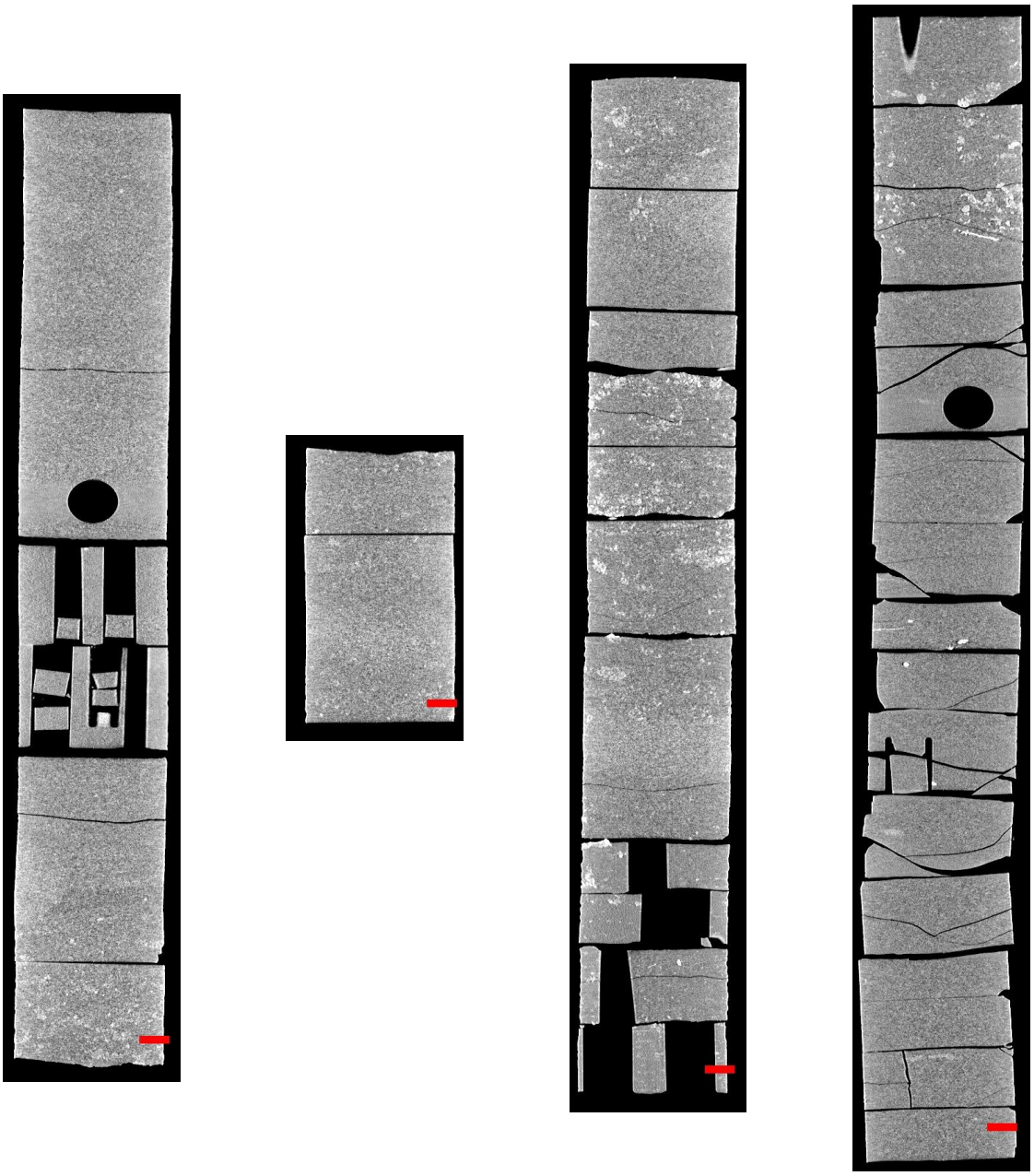

2,930–2,932 ft **2,932–2,934 ft** **2,934–2,937 ft** **2,937–2,940 ft**

Figure 22: 2D midplanes of the medical CT scans of the LG #1 core from 2,930–2,940 ft.

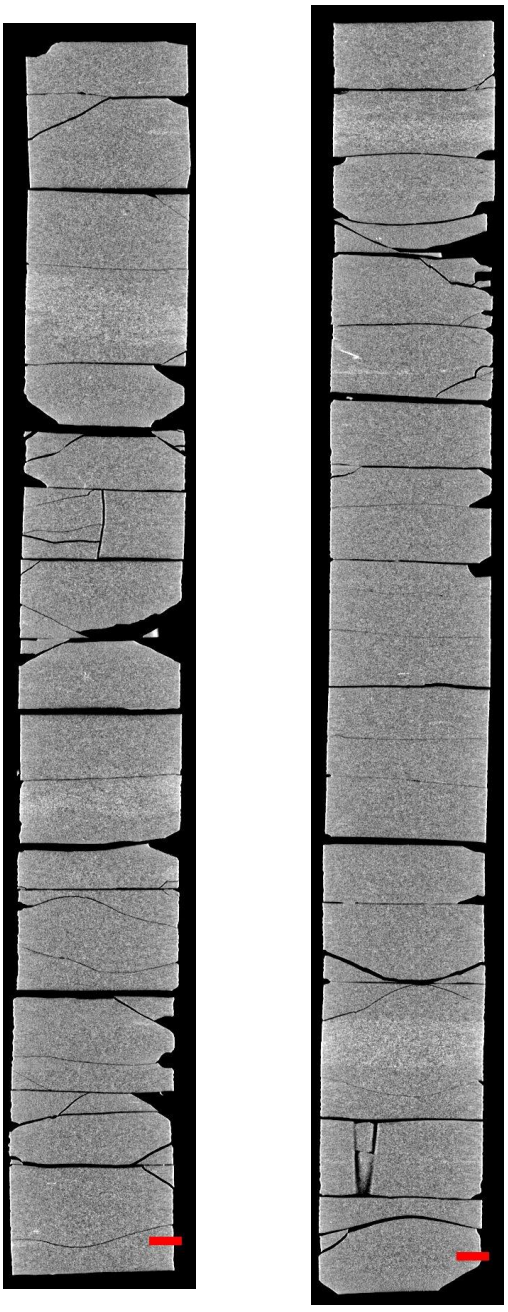

2,940–2,943 ft **2,943–2,945 ft**

Figure 23: 2D midplanes of the medical CT scans of the LG #1 core from 2,940–2,945 ft.

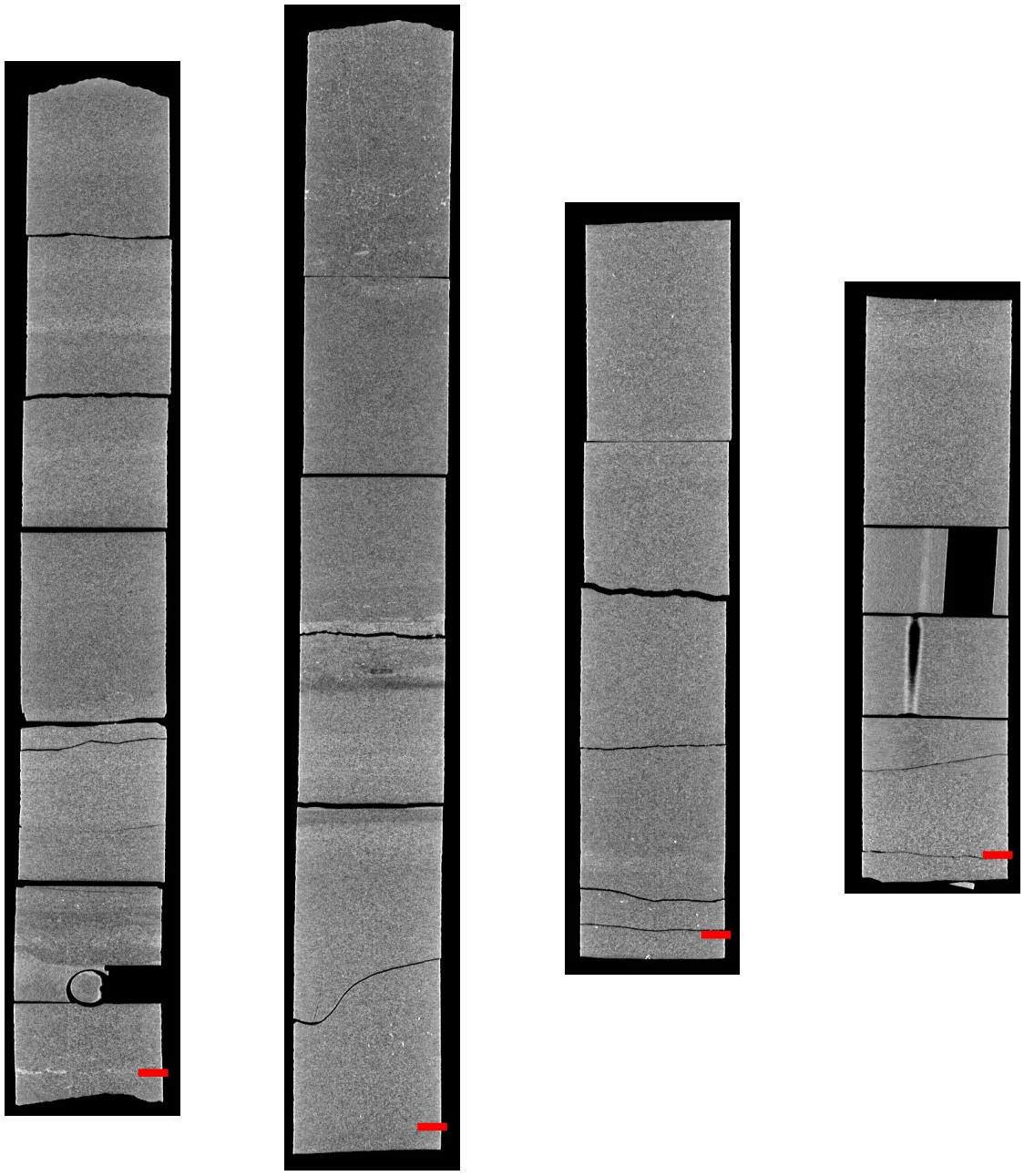

3,570–3,752 ft **3,572–3,575 ft** **3,575–3,577 ft** **3,577–3,578 ft**

Figure 24: 2D midplanes of the medical CT scans of the LG #1 core from 3,570–3,578 ft.

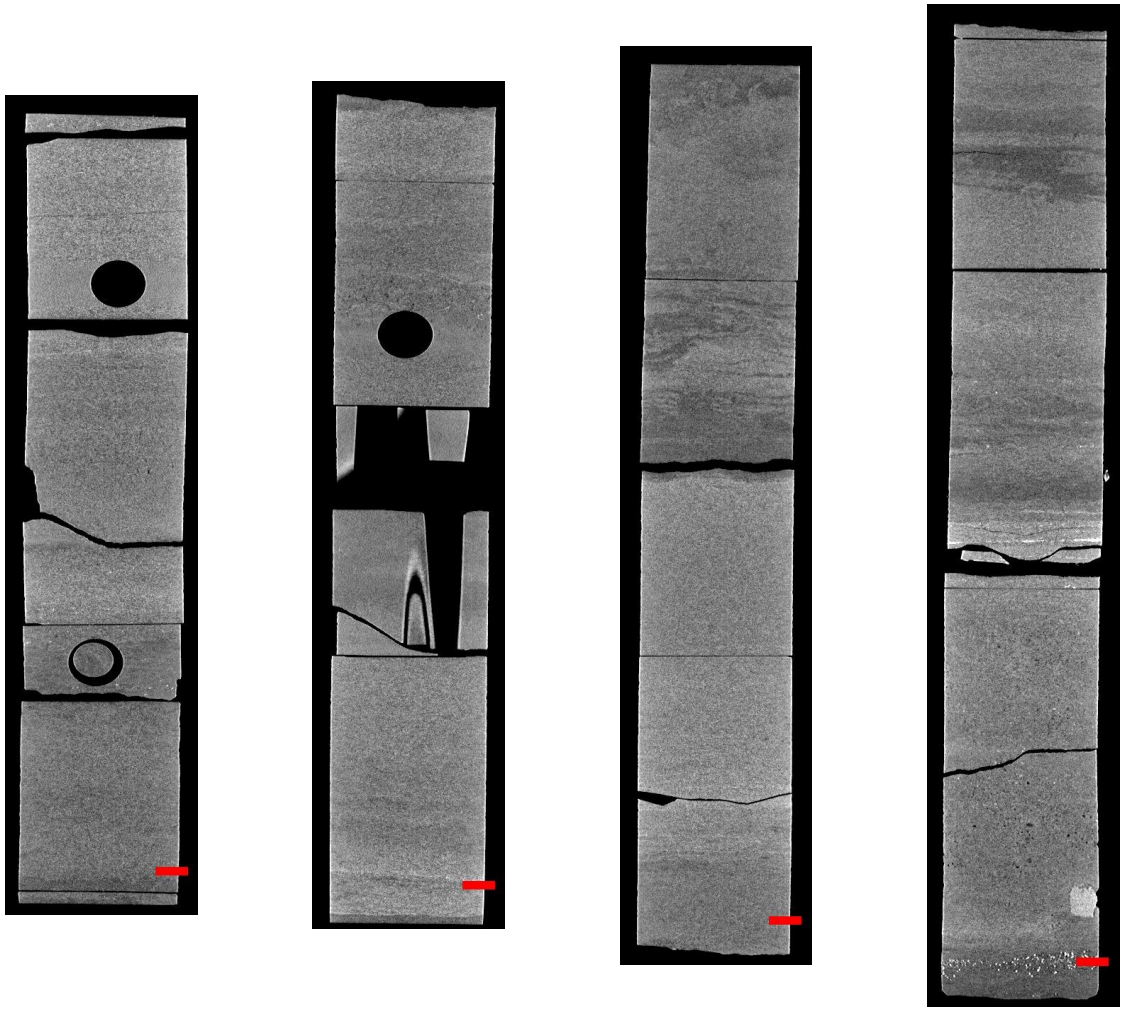

3,578–3,580 ft **3,580–3,582 ft** **3,582–3,584 ft** **3,584–3,587 ft**

Figure 25: 2D midplanes of the medical CT scans of the LG #1 core from 3,578–3,587 ft.

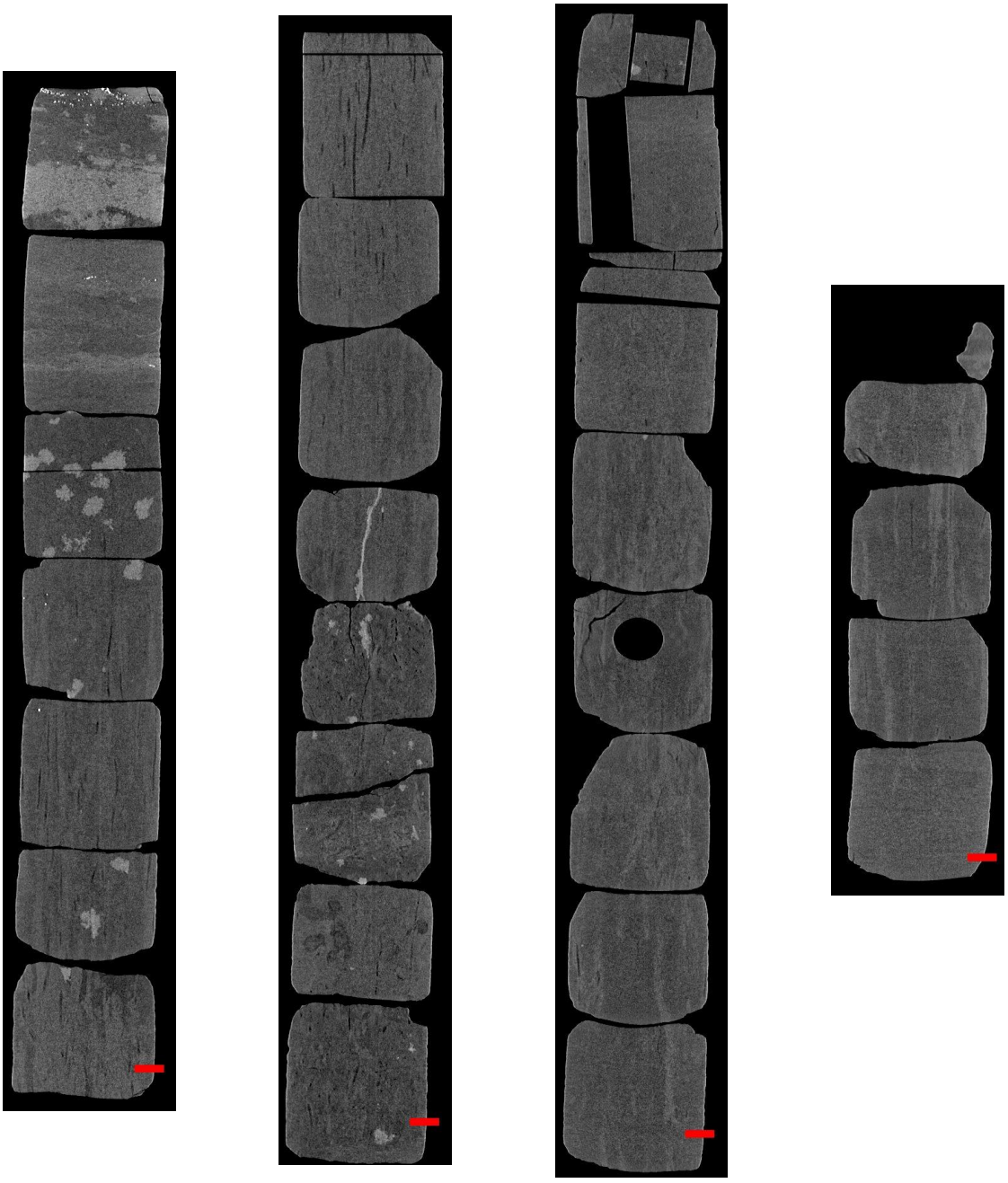

3,587–3,589 ft **3,589–3,592 ft** **3,592–3,595 ft** **3,595–3,597 ft**

Figure 26: 2D midplanes of the medical CT scans of the LG #1 core from 3,587–3,597 ft.

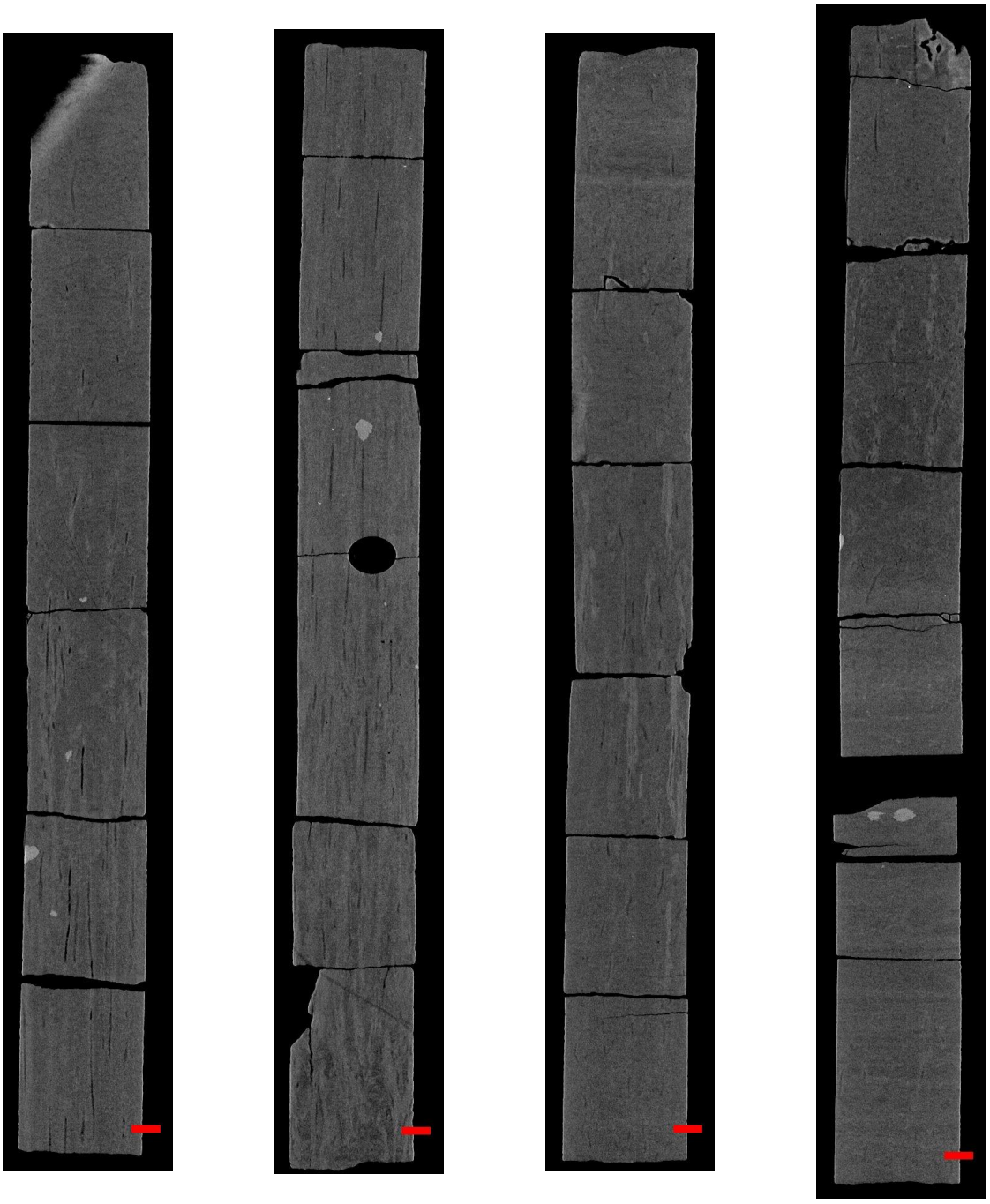

3,649–3,651 ft **3,651–3,654 ft** **3,654–3,657 ft** **3,657–3,660 ft**

Figure 27: midplanes of the medical CT scans of the LG #1 core from 3,649–3,660 ft.

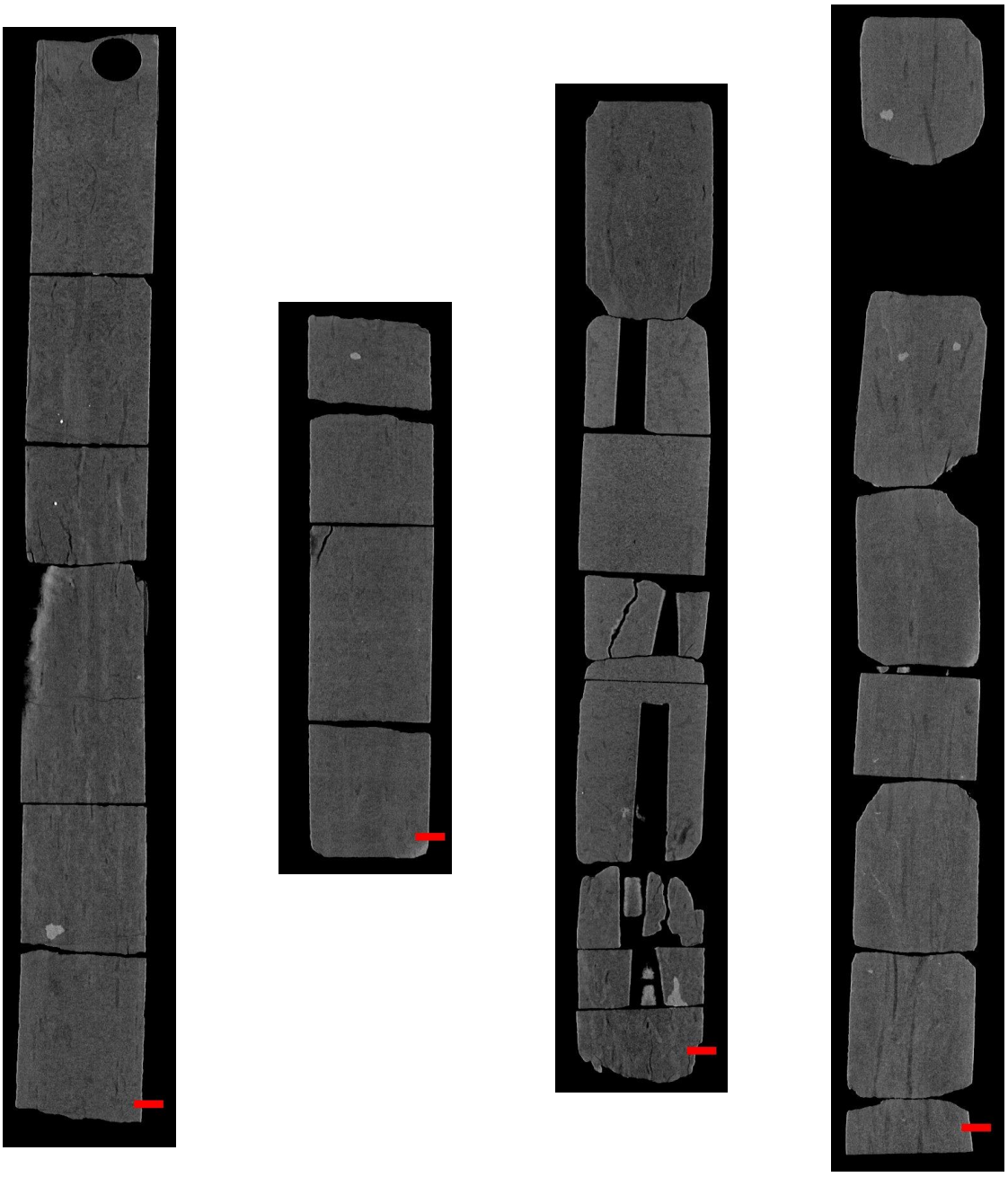

3,660–3,663 ft **3,663–3,665 ft** **3,665–3,667 ft** **3,667–3,670 ft**

Figure 28: 2D midplanes of the medical CT scans of the LG #1 core from 3,660–3,670 ft.

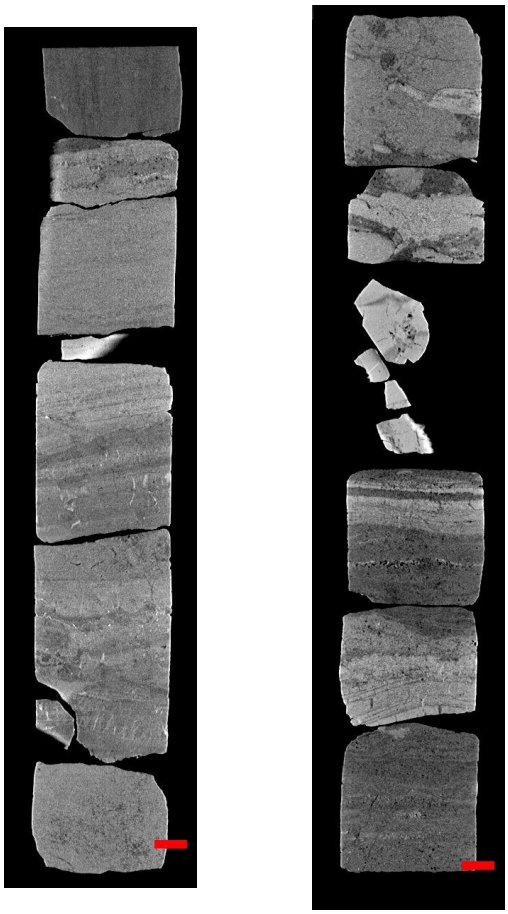

3,670–3,672 ft **3,672–3,674 ft**

Figure 29: 2D midplanes of the medical CT scans of the LG #1 core from 3,670–3,674 ft.

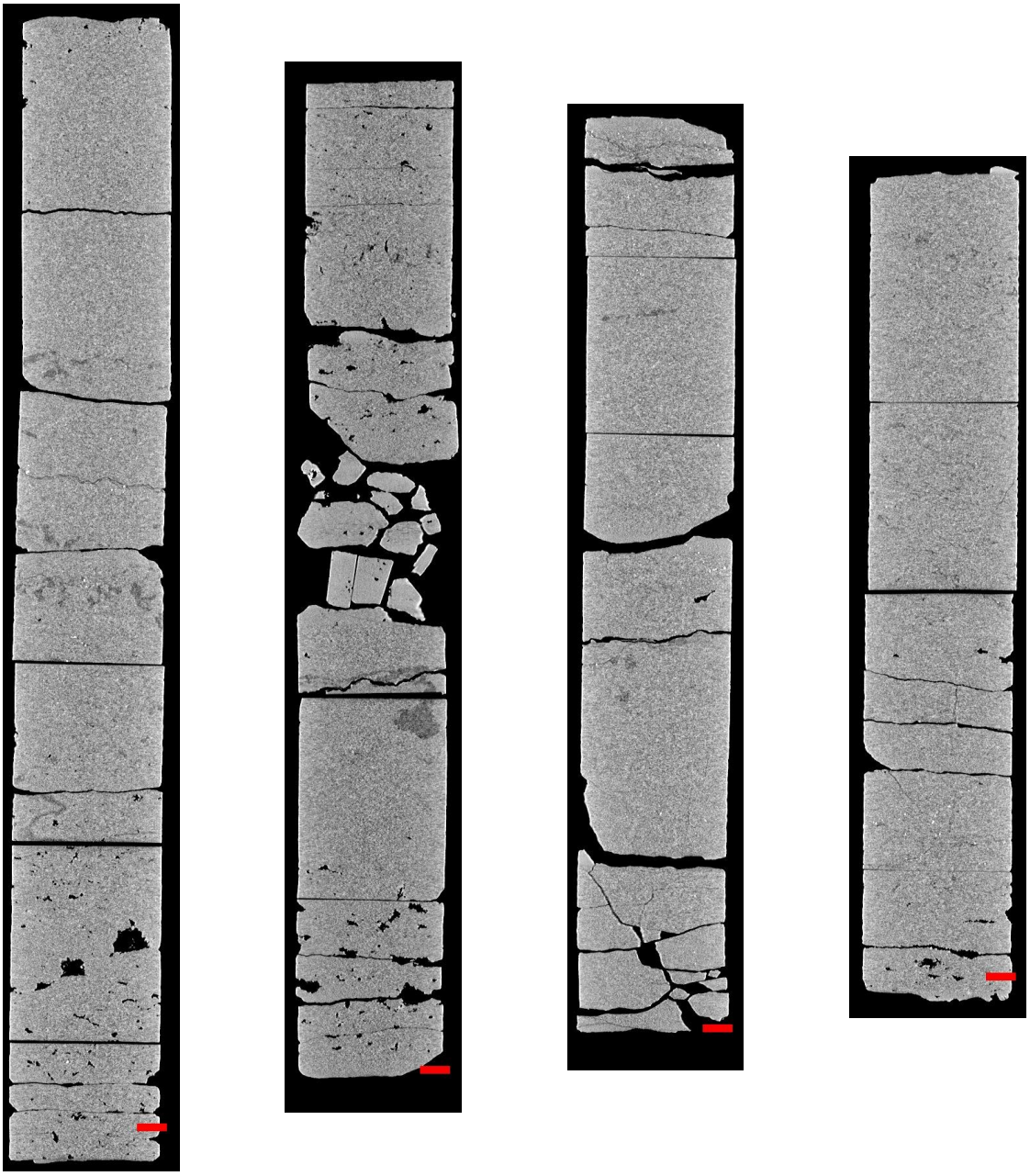

4,885–4,888 ft **4,888–4,890 ft** **4,890–4,893 ft** **4,893–4,895 ft**

Figure 30: 2D midplanes of the medical CT scans of the LG #1 core from 4,885–4,895 ft.

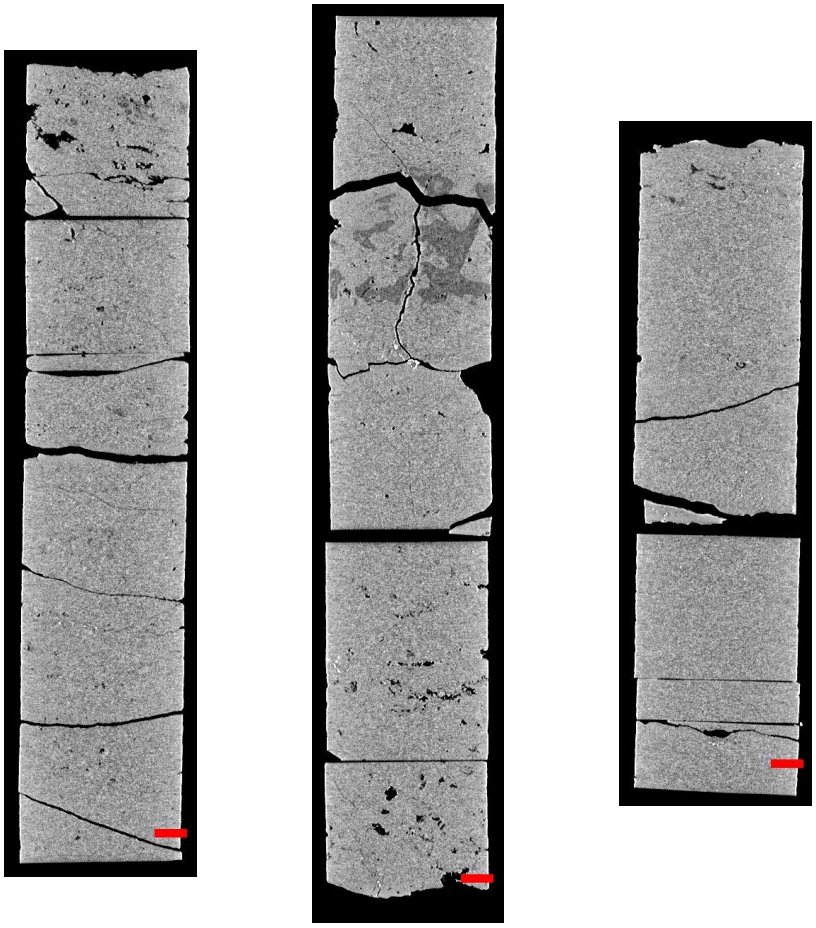

4,895–4,897 ft **4,897–4,899 ft** **4,901–4,903 ft**

Figure 31: 2D midplanes of the medical CT scans of the LG #1 core from 4,895–4,903 ft.

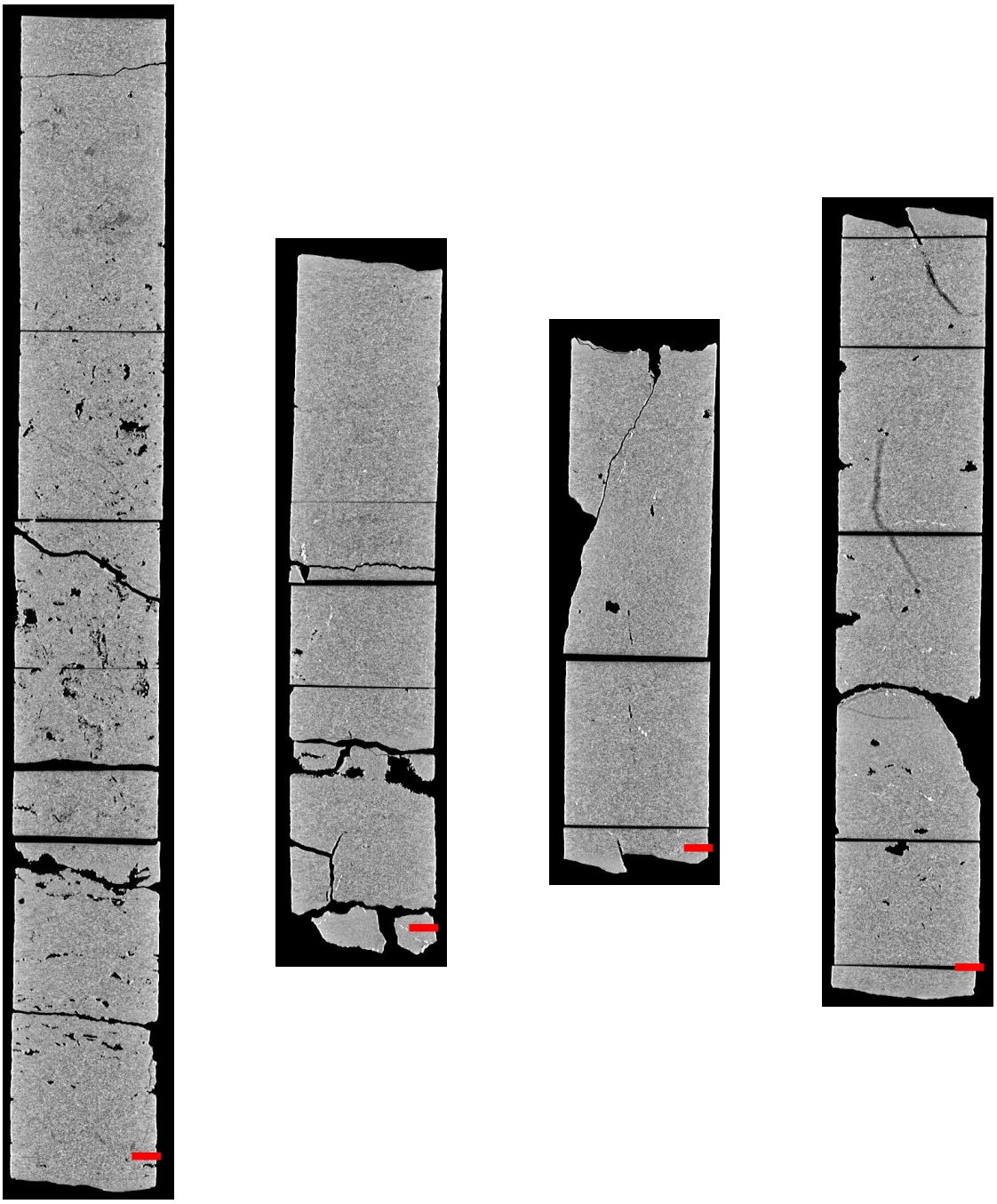

4,903–4,906 ft **4,906–4,908 ft** **4,908–4,909 ft** **4,909–4,911 ft**

Figure 32: 2D midplanes of the medical CT scans of the LG #1 core from 4,903–4,911 ft.

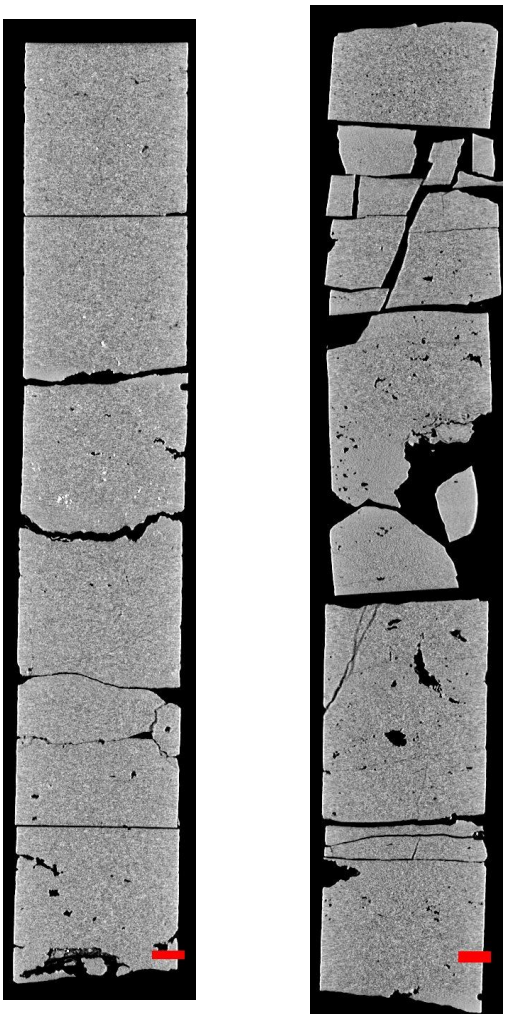

5,295–5,297 ft **5,301–5,304 ft**

Figure 33: 2D midplanes of the medical CT scans of the LG #1 core from 5,295–5,297 ft and 5,301–5,304 ft.

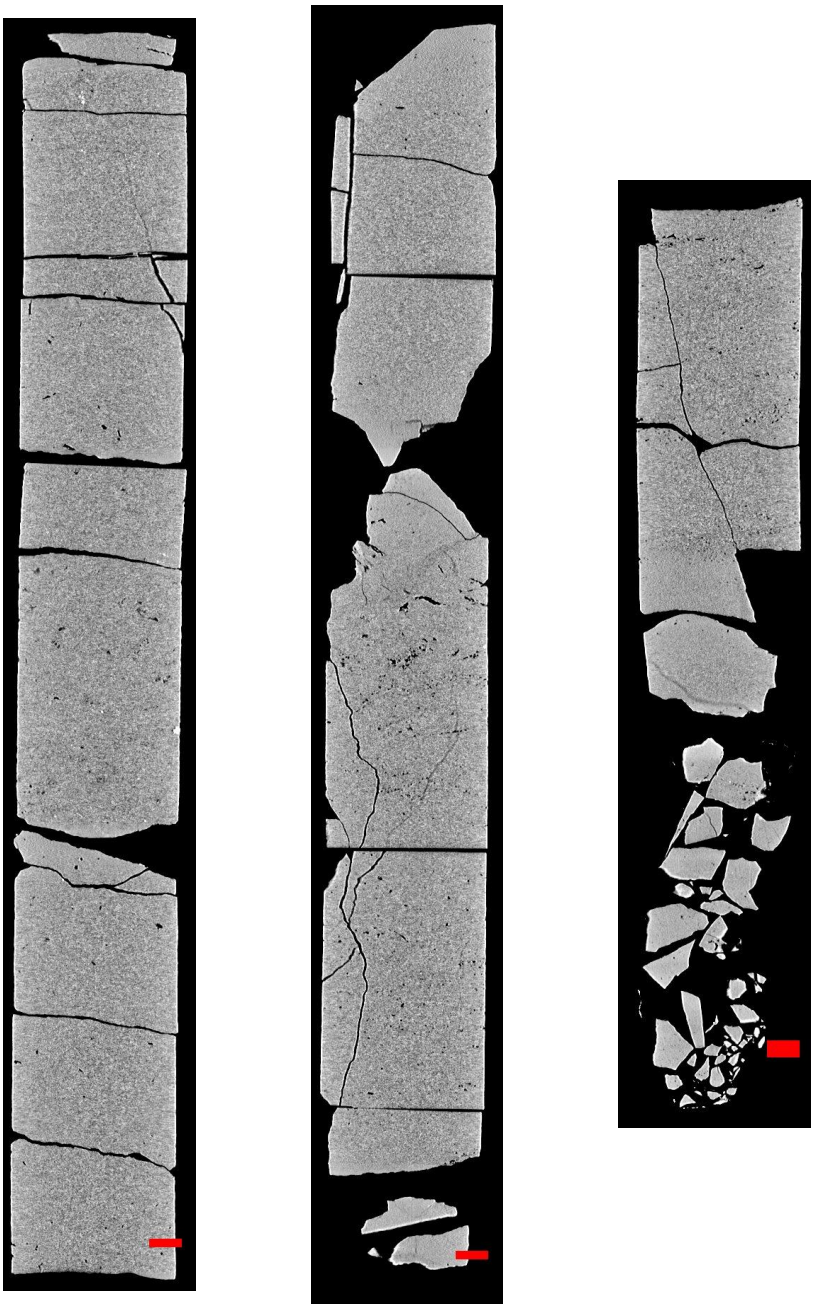

5,305–5,308 ft **5,311–5,314 ft** **5,314–5,315 ft**

Figure 34: 2D midplanes of the medical CT scans of the LG #1 core from 5,305–5,308 ft and 5,311–5,315 ft.

4,895–4,900 ft **4,900–4,905 ft** **5,304–5,309 ft** **5,309–5,314 ft**

Figure 35: 2D midplanes of the medical CT scans of the LG #1 1/3rd slabbed core from 4,895-4,905 ft and 5,309-5,314 ft.

3.2 ADDITIONAL CT DATA

Additional CT data can be accessed from NETL's EDX online system using the following link: https://edx.netl.doe.gov/dataset/isgs-carbonsafe-lively-grove-core. The original CT data is available as 16-bit tif stacks suitable for reading with ImageJ (Schneider et al., 2012) or other image analysis software.

3.2.1 Medical CT Image Videos

In addition, videos showing the variation along the length of the cross-section images shown in the previous section are available for download and viewing on EDX. A single image from these videos is shown in Figure 36, where the cross-section of St. Peter Sandstone displays prominent vertical burrowing. The red line through the XZ-plane image of the core shows the location of the XY-plane displayed above. The videos on EDX show this XY variation along the entire length of the core.

Figure 36: Single image from a video file available on EDX showing variation in the LG #1 core from 3,665–3,667 ft. Image above shows the variation in composition within the matrix perpendicular to the core length.

3.2.2 Industrial CT Scans

Detailed industrial CT scans of core sections were performed at NETL. The industrial CT scanner was used to obtain higher resolution images with voxel resolutions between 67 and 18 μm^3 and capture the details of internal features clearly. A listing of the core sections scanned with the industrial CT scanner is shown in Table 2, followed by XZ reslices of images through the center of these scans. The "File Name" listed in in Table 2 aligns with the naming sequence of data on EDX, where the full scans are available for download and additional analyses. The reslices shown in Figure 37 to Figure 42, are cross-sections through the center of each core to illustrate the internal variation in each sample. Note that the scan of the core from 3,574.2 ft has a 2.59 mm gap between the top and bottom portions due to a scanning error.

Table 2: Industrial Scans of Whole Core

Depth (ft)	File Name	Resolution (μm^3)
2,889	Lively Grove_2889	57.4
2,896	Lively Grove_2896	57.4
2,926.1	LivelyGrove_2926.1	18.8
3,574.2	LivelyGrove_3574.2	18.8
3,584.4	LivelyGrove_3584.4	29.1
3,594	Lively Grove_3594	57.4
3,651.88	LivelyGrove_3651.88	18.8
3,659	LivelyGrove_3659	18.8

Depth (ft)	File Name	Resolution (μm^3)
3,667	Lively Grove_3667	62.5
3,671.5	Lively Grove_3671.5	57.4
4,882.5	Lively Grove_4882.5	62.5
4,895	Lively Grove_4895	62.5
4,904	Lively Grove_4904	62.5
4,904.5	Lively Grove_4904.5	62.5
4,906	LivelyGrove_4906	22.6
5,306	Lively Grove_5306	62.5

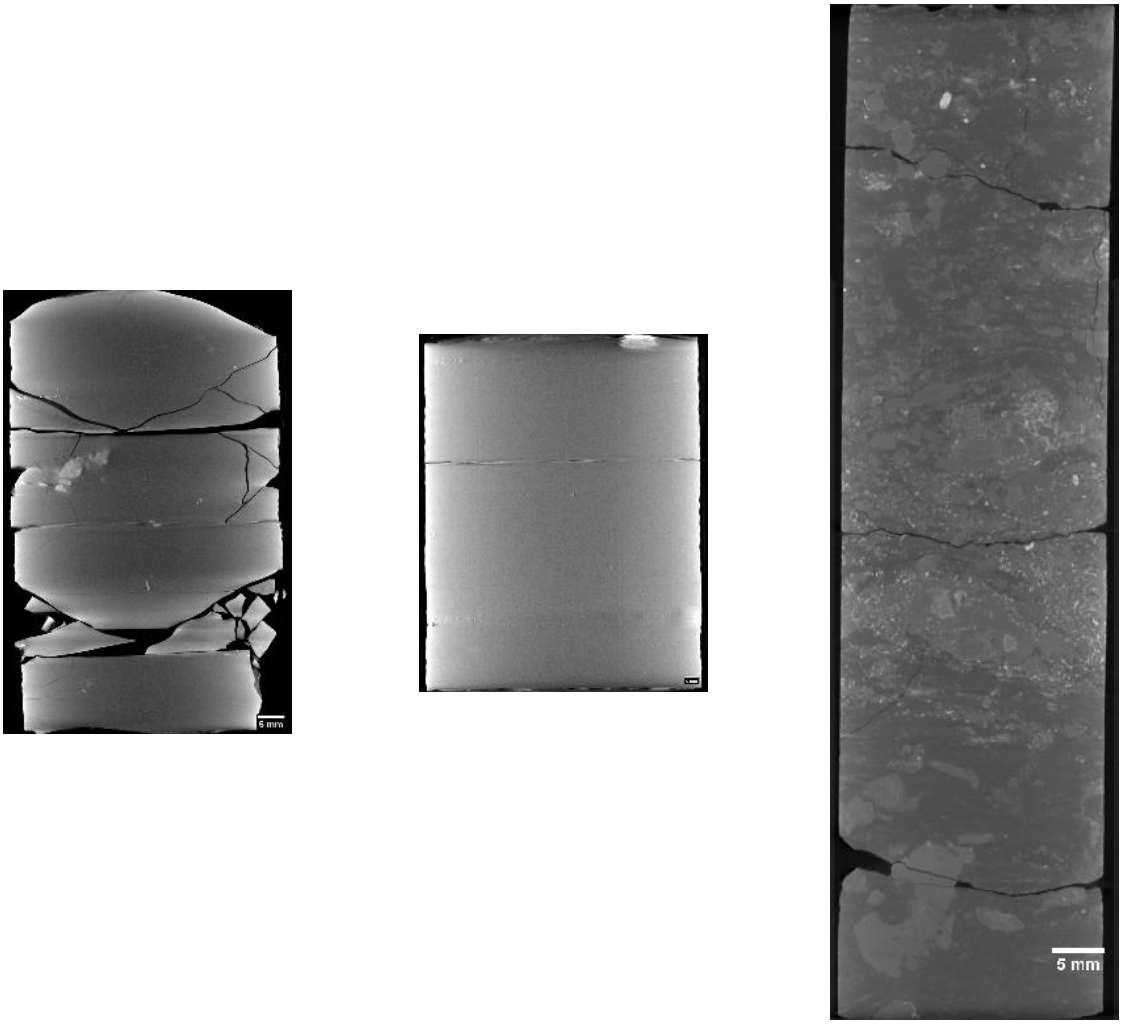

2,889 ft **2,896 ft** **2,926.1 ft**

Figure 37: LG #1 industrial CT scanner images from 2,889 to 2,926.1 ft.

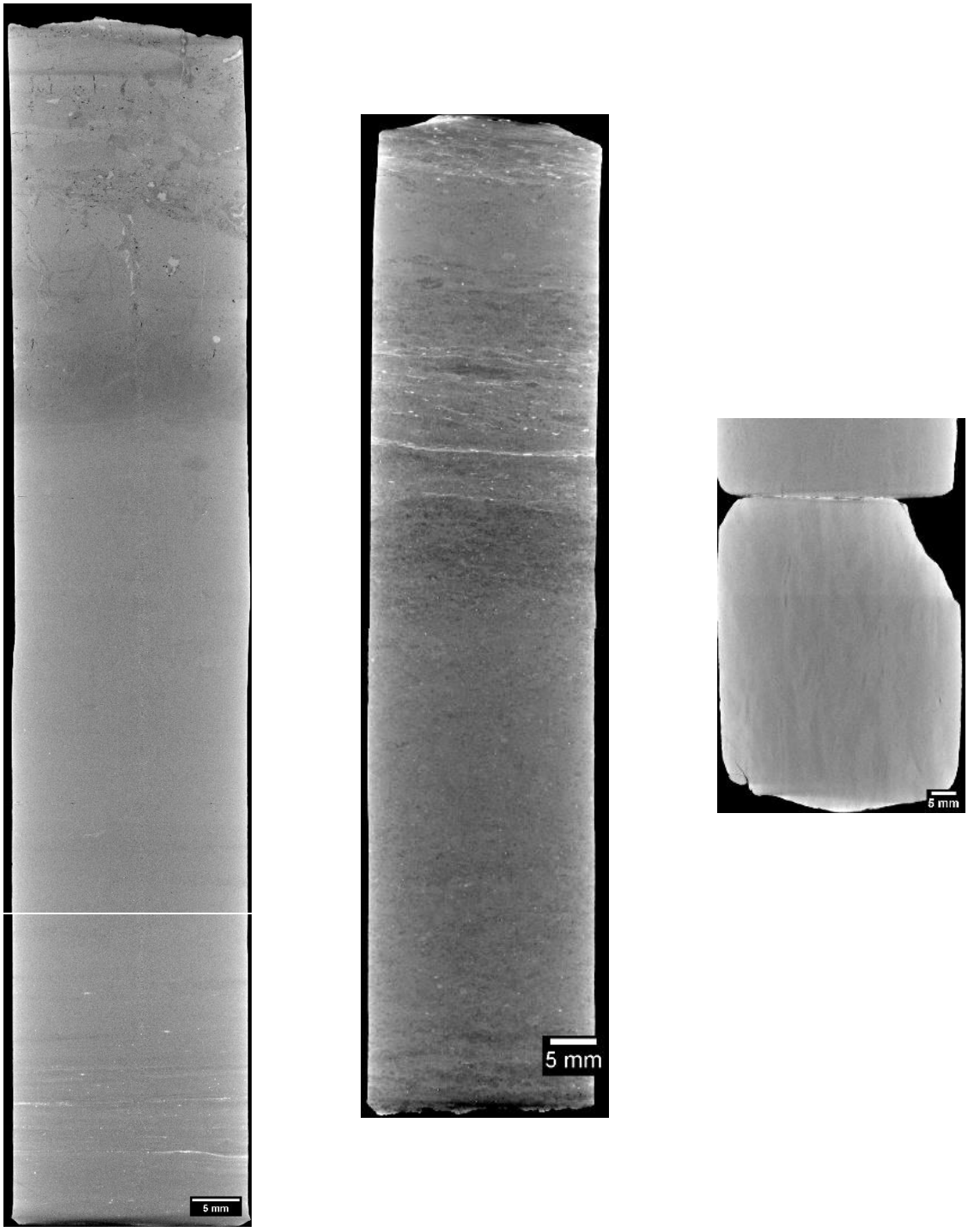

3,574.2 ft **3,584.4 ft** **3,594 ft**

Figure 38: LG #1 industrial CT scanner images from 3,574.2 to 3,594 ft.

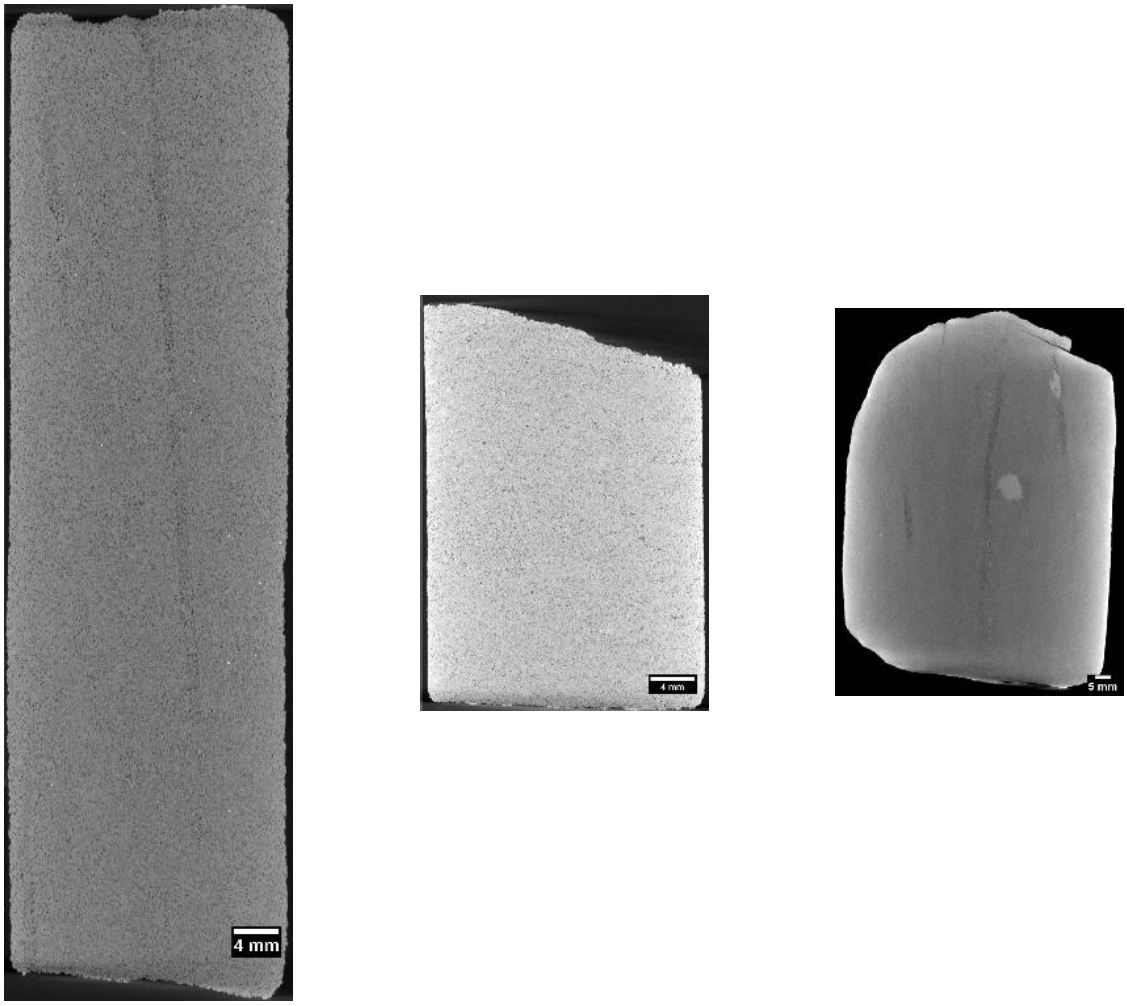

3,651.88 ft **3,659 ft** **3,667 ft**

Figure 39: LG #1 industrial CT scanner images from 3,651.88 to 3,667 ft.

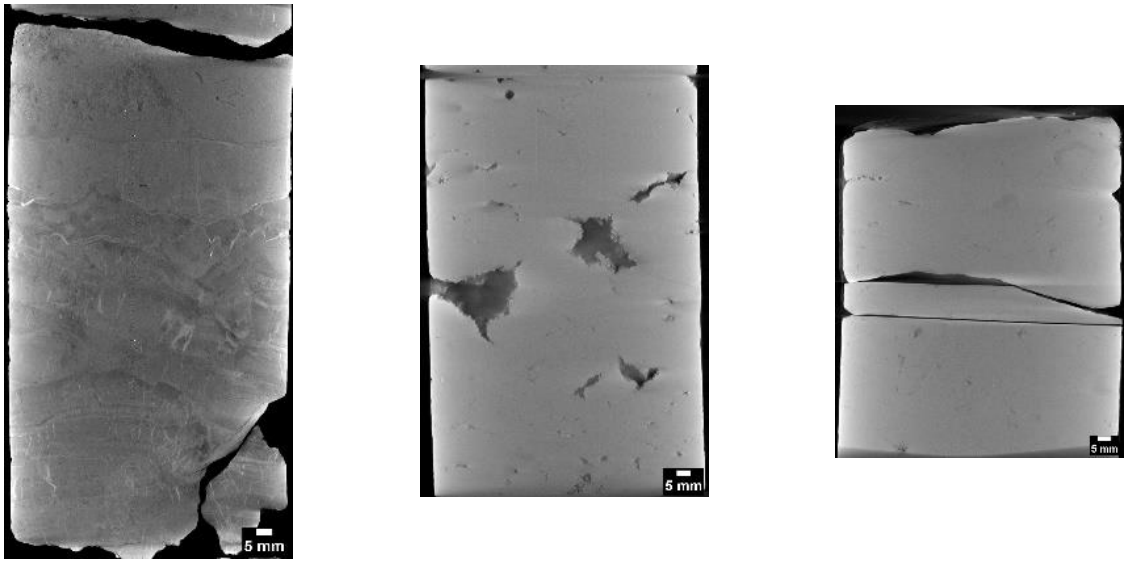

3,671.5 ft **4,882.5 ft** **4,895 ft**

Figure 40: LG #1 industrial CT scanner images from 3,671.5 to 4,895 ft.

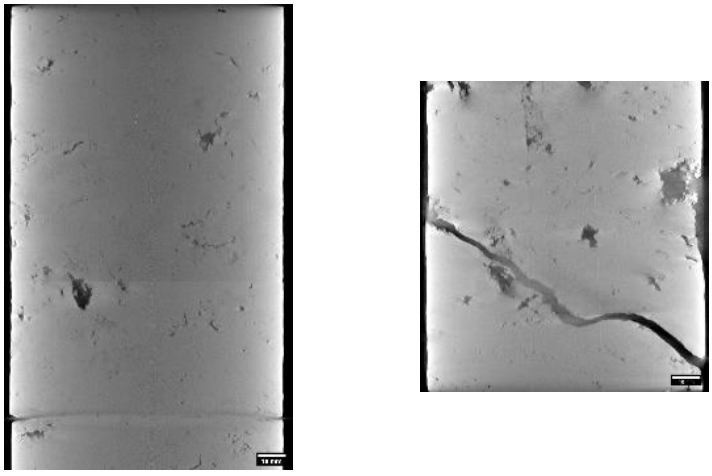

4,904 ft **4,904.5 ft**

Figure 41: LG #1 industrial CT scanner images from 4,904 and 4,904.5 ft.

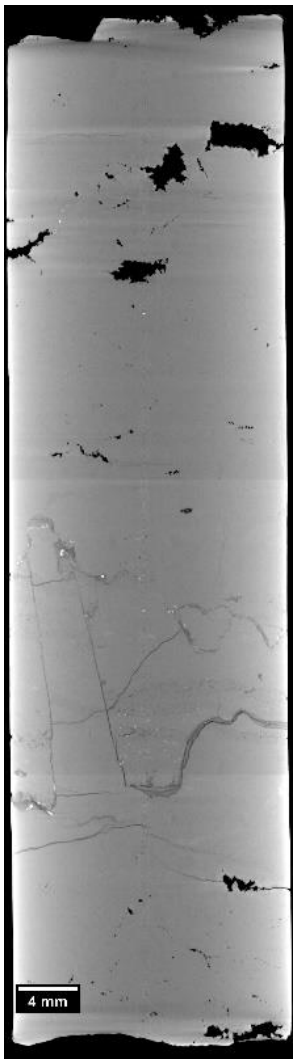

4,906 ft **5,306 ft**

Figure 42: LG #1 industrial CT scanner images from 4,906 and 5,306 ft.

3.2.3 Micro CT scanning

Detailed scans of the section of interest were preformed using NETL's Xradia CT scanner and DynaTOM scanner. Table 3 lists the selected intervals with depth and voxel resolution for each scanner. An example of the micro CT images are shown in montage images in Figure 43 to Figure 49, where each image is an isolated slice along the length of the core; note each scale bar represents 0.5 cm.

Table 3: Micro CT Images from the ZEISS Xradia MicroXCT-400 and DynaTOM Scanners

Depth (ft)	Name	Voxel Resolution (μm^3)
3,571.6	Xradia - Lively Grove 3571.6	1.87
3,590.0	Xradia - Lively Grove 3590.0	1.87
3,660.0	Xradia - Lively Grove 3660.0 10x	1.51
3,667	Xradia - Lively Grove 3667.0	1.47
3,674	Xradia - Lively Grove 3674.0	1.47
3,665.21	DynaTOM - Lively Grove 3665.21	23.4

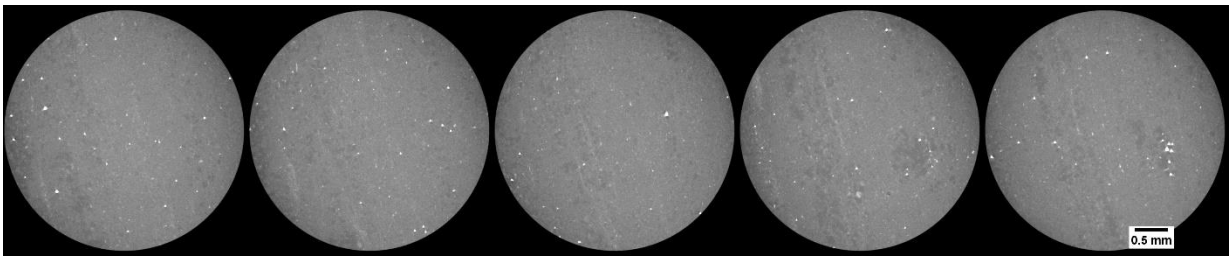

Figure 43: Micro-CT images from the LG #1 core at a depth of 3,571.6 ft.

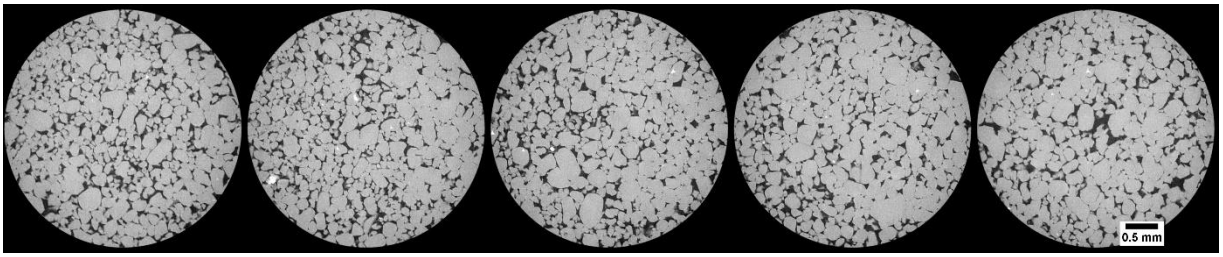

Figure 44: Micro-CT images from the LG #1 core at a depth of 3,590 ft.

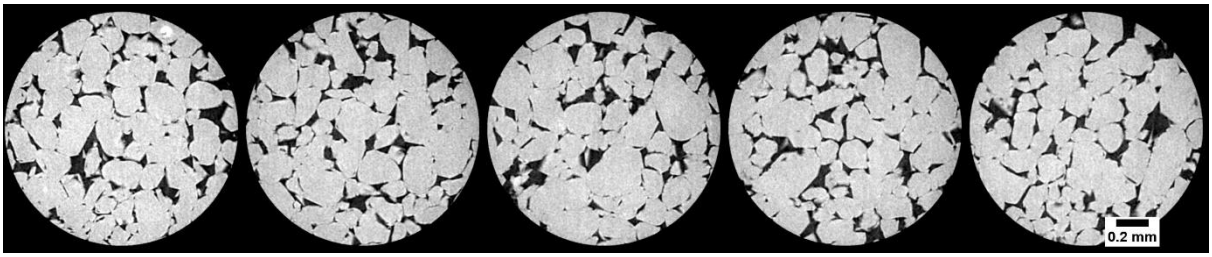

Figure 45: Micro-CT images at 10x resolution from the LG #1 core at a depth of 3,660 ft.

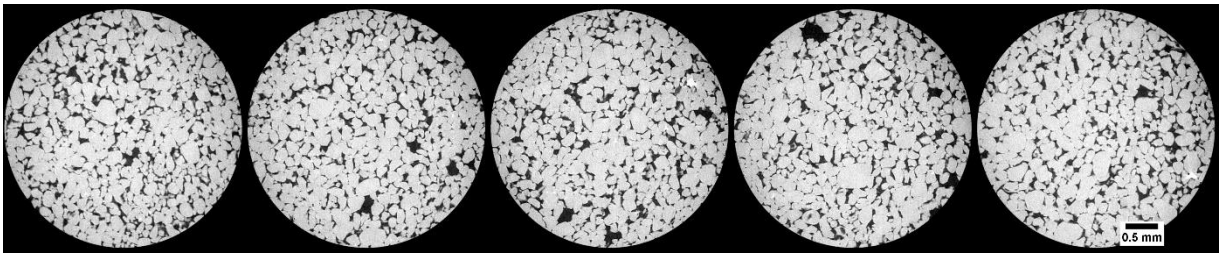

Figure 46: Micro-CT images from the LG #1 core at a depth of 3,660 ft.

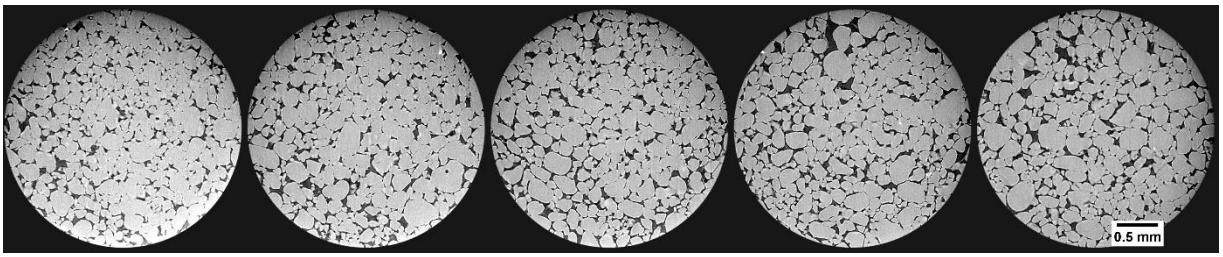

Figure 47: Micro-CT images from the LG #1 core at a depth of 3,667 ft.

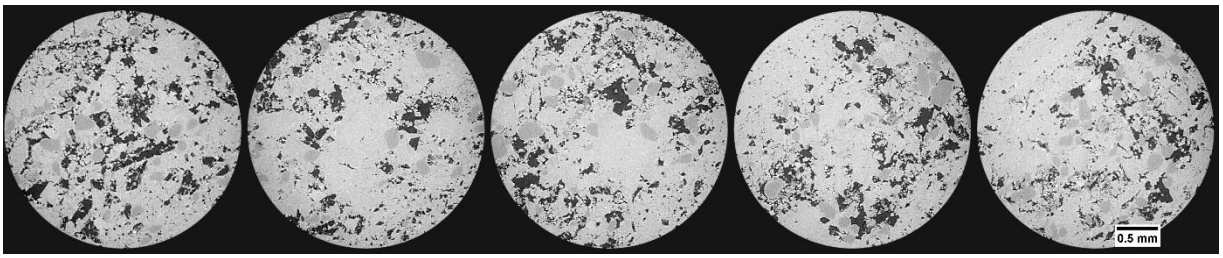

Figure 48: Micro-CT images from the LG #1 core at a depth of 3,674 ft.

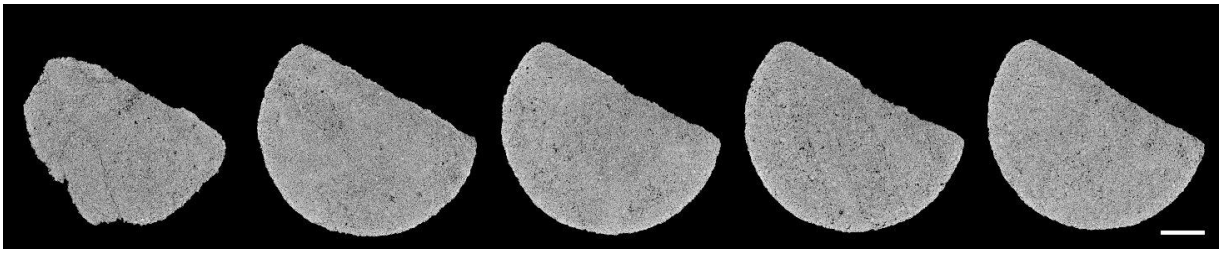

Figure 49: Micro-CT images from the LG #1 core at a depth of 3,665.21 ft.

3.3 DUAL ENERGY CT SCANNING

Dual energy CT scanning uses two sets of images, produced at different X-ray energies, to approximate the density (ρ_B) (Siddiqui and Khamees, 2004; Johnson, 2012). The technique relies on the use of several standards of known ρ_B to be scanned at the same energies as the specimen. These scans are performed at lower energies (<100 KeV) and higher energies (>100 KeV) to induce two types of photon interactions with the object (Figure 50). The lower energy scans induce photoelectric absorption, which occurs when the energy of the photon is completely absorbed by the object mass and causes ejection of an outer orbital electron (Figure 50a). The high energy scans induce Compton scattering, which causes a secondary emission of a lower energy photon due to incomplete absorption of the photon energy in addition to an electron ejection (Figure 50b).

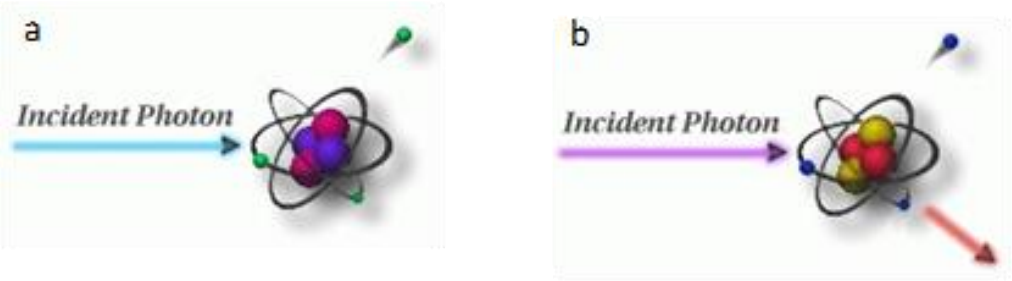

Figure 50: Photon interactions at varying energies: a) Photoelectric absorption, b) Compton scattering. Modified from Iowa State University Center for Nondestructive Evaluation (2021).

Medical grade CT scanners are typically calibrated to known standards, with the output being translated in CTN or Hounsfield Units (HU). Convention for HU defines water as 0 and air as -1,000. A linear transform of recorded HU values is performed to convert them into CTN. This study used CTN as it is the native export format for the medical CT scanner, but it is possible to use HU. Dual energy CT requires at least three calibration points, and it is prudent to utilize standards that approximate the object or material of interest. Pure samples of aluminum, graphite, and sodium chloride were used as the calibration standards as they most closely approximate the rocks and minerals of interest (Table 4). Most materials denser than water or with higher atomic masses have a non-linear response to differing CT energies (Table 5).

Table 4: Dual Energy Calibration Standards, Bulk Density (gm/cm^3)

Material	ρ_B (g/cm^3)
Air	-0.001
Water	1
Graphite	2.3
Sodium Chloride	2.16
Aluminum	2.7

Table 5: Dual Energy Calibration Standards, HU and CTN for "Low" and "High" Energies

Material	HU		CTN	
	80 KeV	135 KeV	80 KeV	135 KeV
Air	-993	-994	31,775	31,774
Water	-3.56	-2.09	32,764	32,766
Graphite	381	437	33,149	33,205
Sodium Chloride	1,846	1,237	34,614	34,005
Aluminum	2,683	2,025	35,451	34,793

Dual energy CT utilizes these differences to calibrate to the X-ray spectra. Two equations with three unknowns each are utilized to find ρ_B (Siddiqui and Khamees, 2004):

$$\rho_B = mCTN_{low} + pCTN_{high} + q$$

Where [m, p, and q] are unknown coefficients that can be solved by setting up a system of equations with four 3 x 3 determinants. The CTN is obtained from the CT scans for each of the homogenous calibration standards.

In this study, the high and low energy image stacks were loaded into Python as arrays. A 3D Gaussian blur filter with a sigma of 2 was used to reduce noise in the images. The scipy.solv module of Python was then employed to solve for the coefficients based on the calibration CTN values. The ρ_B was solved for each pixel in the 3D volume and saved as two new separate image stacks.

3.4 COMPILED CORE LOG

The compiled core logs were scaled to fit on single pages for rapid review of the combined data from the medical CT scans and MSCL readings. Logs are presented for each of the cored sections in the Maquoketa, Joachim and St. Peter, and Knox Megagroup (noted in figure

captions). Due to core loss during transportation some intervals are missing data. To get the best data coverage possible, the 2/3rd slabbed cores were used to measure gamma density, and p-wave velocity (not displayed); 1/3rd slabbed cores were used to measure magnetic susceptibility and elemental composition using XRF. All available cores were medically CT scanned. Each log includes the following tracks: track 1, gamma density and dual energy density; track 2, magnetic susceptibility; track 3, medical CT images, cropped to center portion of images to highlight greyscale variations; track 4, elemental XRF mineralogy that are colored to indicate carbonates (blue, Mg + Ca), quartz (yellow, Si), and clays (grey, Al; red, Fe; pink, K); tracks 5, 6, 7, and 8 proxy elemental measurements in parts per million; and tracks 9 and 10 contain elemental ratios.

The elemental results from the XRF was used to display important elemental proxies related to detrital influence (Si, Al, K, Ti, and Zr in track 5), skeletal influx/carbonate potential (Ca, Mg, Mn, and Ba in track 6), redox potential (V, Cr, Co, Ni, Cu, and Mo in track 7), and biogenic production (V, P, Zn, and Y in track 8).

Trends in elemental ratios can provide insight to variations in mineral composition, oxidation state, and depositional setting. Seven elemental ratios are displayed in tracks 9 and 10. A short description of how these are representative of various geological processes are listed in Table 6.

Table 6: Elemental Ratio Descriptions

Elemental Ratio	Marker for:	Lower Value	Higher Value
Si/Al	Abundance of illite and micas versus other clays	More of other clay types	More illite and micas
Ti/Al	Terrigenous input	Less eroded content	More eroded content
Ca/Mg	Dolomite	More dolomitic	Less dolomitic
Ca/Si	Relative abundance of calcium carbonates versus silicates	Silicate rich	Carbonate rich
S/Fe	Abundance of pyrite (and other iron sulfates) vs. other Fe oxide metals	Fe-oxide dominate/ sulfate lean	Sulfate rich
Fe/Al	Degree of pyritization in shales	Lower degree of pyritization	Higher degree of pyritization
Mn/Fe	Oxidation	More anoxic/euxinic	More dysoxic/oxic

The elemental proxy log also includes an XRF “mineralogy” with Al and K, representing clays; Ca, representing calcite; and Si, representing quartz, although there is some Si contribution to the clays. Pyrite (reduced) should have low magnetic susceptibility, and Fe oxide or hydroxide should have high magnetic susceptibility. These broad trends can quickly give information over large lengths of core and direct more focused research to zones of potential interest. These logs are presented in the following images (Figure 51 to Figure 53).

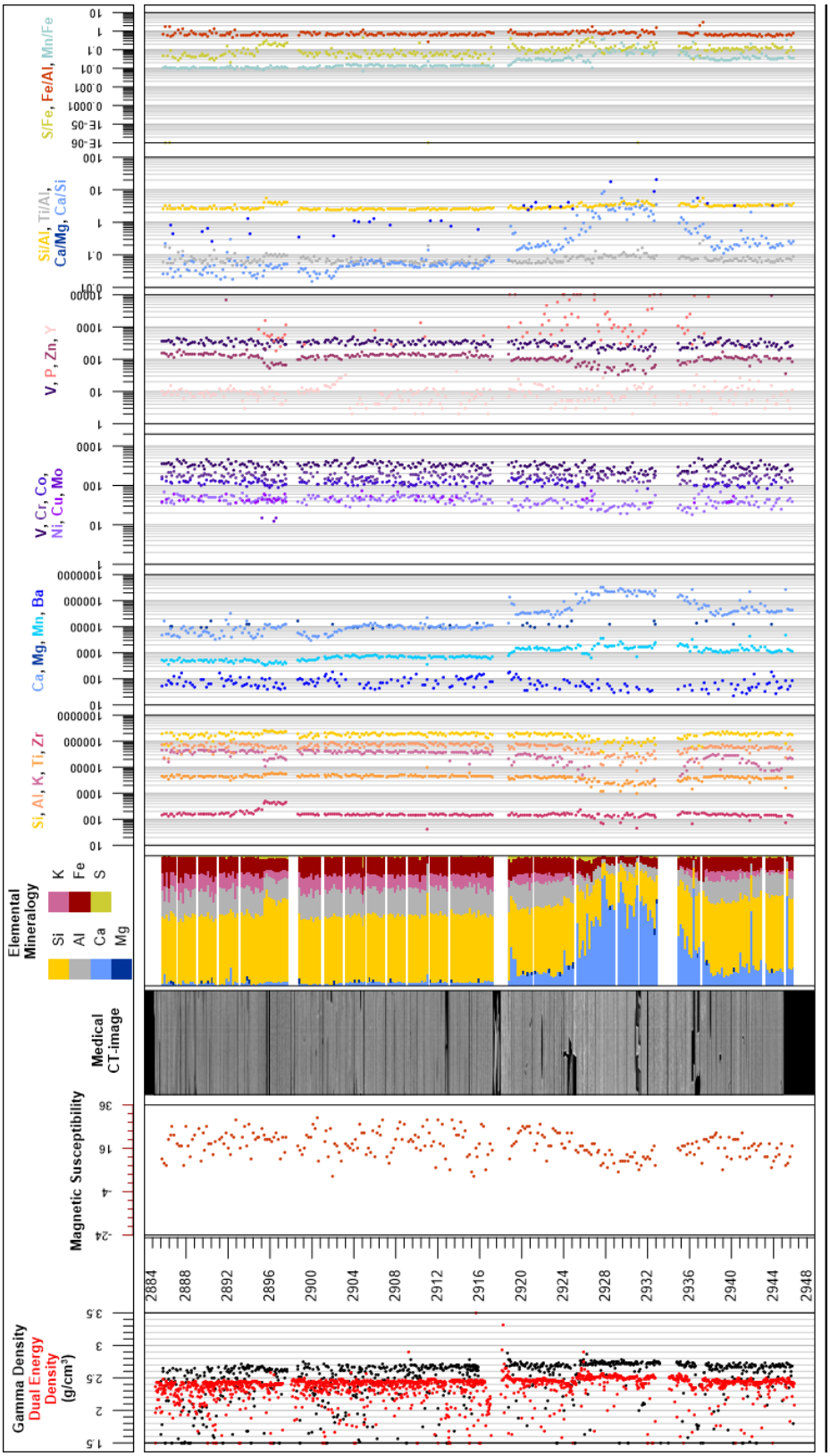

Figure 51: Compiled core log for Lively Grove #1 Well, Maquoketa from 2,885–2,945.8 ft.

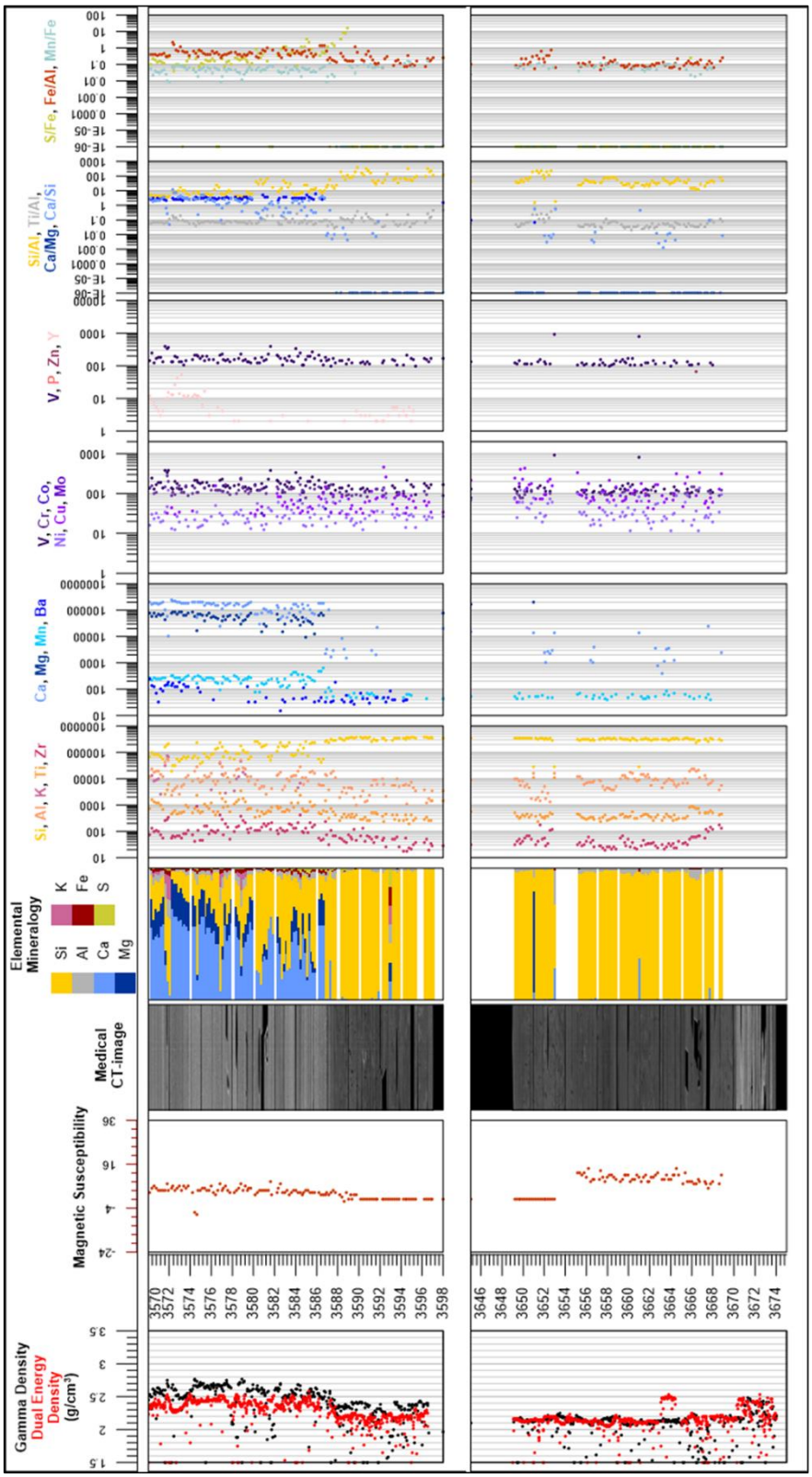

Figure 52: Compiled core log for Lively Grove #1 Well, Joachim and St. Peter Fm. from 3,570–3,675 ft.

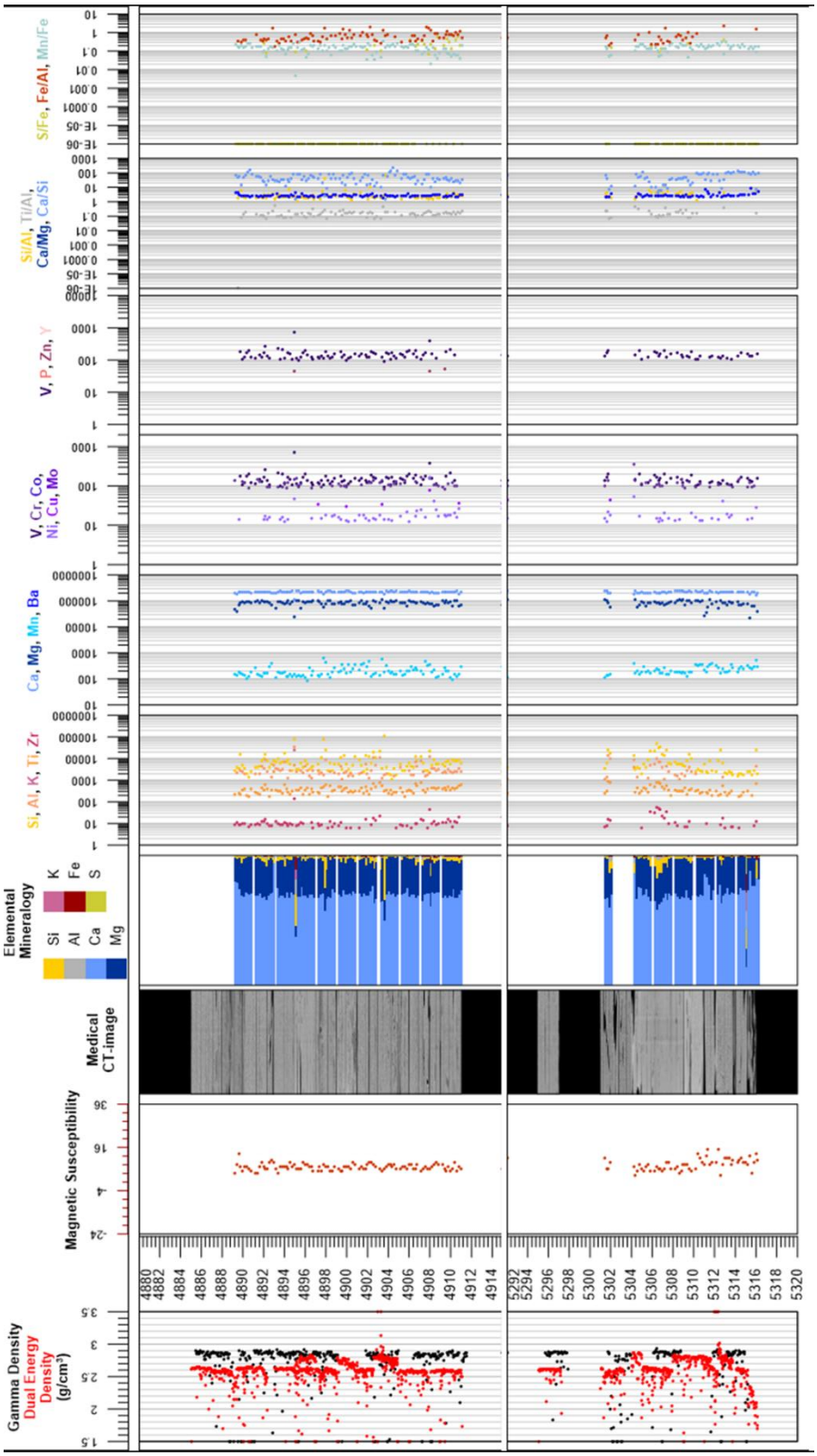

Figure 53: Compiled core log for Lively Grove #1 Well, Knox Dolomite from 4,885–4,912 ft, and 5,294–5,317 ft.

4. DISCUSSION

The evaluation of the magnetic susceptibility, elemental XRF, and CT analysis offers a unique look into the internal structure of the core and macroscopic changes in lithology. These methods:

- Are non-destructive
- When employed together, they offer a more thorough understanding of the core than any single technique alone
- Can be used to identify zones of interest for further detailed analysis, experimentation, and quantification
- Provide a detailed digital record of the core, before any destructive testing or further degradation, that is accessible and can be referenced for future studies

5. REFERENCES

Geotek Ltd. Multi-Sensor Core Logger Manual; Version 05-10; Published by Geotek, 3 Faraday Close, Daventry, Northamptonshire NN11 8RD, 2010. info@geotek.co.uk, www.geotek.co.uk

Hunts, C.; Moskowitz, B.; Banerjee, S. *Magnetic Properties of Rocks and Minerals;* Rock Physics and Phase Relations: A Handbook of Physical Constants; 1995; pp 189–204.

Iowa State University Center for Nondestructive Evaluation, Ames, IA, 2021. https://www.nde-ed.org/Physics/X-Ray/attenuation.xhtml (accessed July 2021).

Johnson, T. R. C. Dual-Energy CT: General Principles. *American Journal of Roentgenology* **2012,** *199*, S3–S8. DOI: 10.2214/AJR.12.9116.

Schneider, C. A.; Rasband, W. S.; Eliceiri, K. W. NIH Image to ImageJ: 25 years of image analysis. *Nature Methods* **2012,** *9*, 671–675.

Siddiqui, S.; Khamees, A. A. Dual-Energy CT-Scanning Applications in Rock Characterization. *Society of Petroleum Engineers* **2004**. DOI:10.2118/90520-MS.

Whittaker, S. Illinois Storage Corridor DE-FE0031892, 2022 Carbon Management Research Project Review Meeting, PA, 2022. (https://netl.doe.gov/sites/default/files/netl-file/22CM_CTS16_Whittaker.pdf).

This page intentionally left blank.

Brian J. Anderson
Director
National Energy Technology Laboratory
U.S. Department of Energy

Darin Damiani
Carbon Storage Program Manager
Office of Carbon Management
U.S. Department of Energy

Mark McKoy
Carbon Storage Technology Director
National Energy Technology Laboratory
U.S. Department of Energy

Bryan Morreale
Executive Director
Research and Innovation Center
National Energy Technology Laboratory
U.S. Department of Energy

NETL Technical Report Series